RSC Advances

Accepted Manuscript

ROYAL SOCIETY OF CHEMISTRY

rsc.li/rsc-advances

RSC Advances

ARTICLE

Experimental and computational studies of protolytic and tautomeric equilibria of Erythrosin B and Eosin Y in water/DMSO

Received 00th January 20xx,
Accepted 00th January 20xx

DOI: 10.1039/x0xx00000x

www.rsc.org/

D. Vanzin[a], C. F. Freitas[a], D. S. Pellosi[a], V. R. Batistela[a], A. E. H. Machado[b], R. M. Pontes[a], W. Caetano[a] and N. Hioka[a]*.

Xanthene dyes Eosin Y (EOS) and Erythrosin B (ERY) are photosensitizers that present complex protolytic system. To understand how the media affects their properties, we correlated the experimental pK_a in water/DMSO with theoretical calculation by molecular modeling approaches based on their tautomer´s energy. It shows that in EOS the phenolic group is more acid than the carboxylic due to the presence of bromine atoms. The iodine in ERY, through the stability of tautomers involved in the protolytic forms, drives $pK_{a\text{-}COOH}<pK_{a\text{-}OH}$ in water-rich media and the inversion $pK_{a\text{-}OH}<pK_{a\text{-}COOH}$ in DMSO-rich media caused by the solvation that affects its tautomeric equilibria. For EOS, the possible protolytic equilibria are: NEL ⇌ MAF or NEQ ⇌ MAF as $pK_{a1}=pK_{a\text{-}OH}$ and MAF ⇌ DA as $pK_{a2}=pK_{a\text{-}COOH}$ in the range of 0 to 70 % of DMSO in water. For ERY at above 35% DMSO in water, the $pK_{a\text{-}OH}<pK_{a\text{-}COOH}$ came from the high amount of MAF and NEL, indicating that these tautomers may be responsible by the inversion. These effects are originated from different electronic delocalization influenced by the overlap between the σ natural bond orbitals of C–I (ERY) or C–Br (EOS) with π* of C–C, higher for ERY than for EOS. The simulated spectra permitted to confirm experimental finds of molar fractions. The analysis of the molecular orbitals confirmed that the main changes in absorption profile are due to HOMO-LUMO π-π* transitions related to the phenolic group. The results allowed the understanding of the influence of environment on preferential tautomers and pK_a.

Introduction

Erythrosin B (Acid Red 51; C.I. 45430; 6-Hydroxy-2,4,5,7-tetraiodofluorescein, named as ERY) and Eosin Y (acid red 87; C.I. 45380; 2,4,5,7-tetrabromofluorescein, named as EOS) are xanthene dyes that generate singlet oxygen with high efficiency, an essential feature for Photodynamic Therapy (PDT) and Photodynamic Inactivation of Microorganisms (PDIMO).[1-7]

However, both ERY and EOS are polyprotic acids and few reports have considered which chemical structure is responsible for their photophysical properties due to their complex dependence with the local pH. Indeed, both dyes present three protolytic groups with close pK_a values. Moreover, each of protolytic specie presents a complex tautomeric equilibria.[8-14]

ERY and EOS compounds present two phenolic groups in the xanthene ring and a carboxylic substituent at the benzene ring. These three pK_a correspond to four protolytic species: the most acid specie is the cationic (CT), followed by the neutral (NE), the monoanionic (MA) and the basic dianionic (DA). However the neutral NE species presents three tautomeric forms, the zwitterionic (NEZ), the quinoid (NEQ) and the lactone (NEL), while the monoanionic (MA) exhibits two tautomers, the carboxylate (MAC) and the phenolate (MAF).[8-12,15,16] Fig. 1 illustrates the structure of these protolytic species and their tautomers.

The presence of each tautomeric form is also dependent on the local polarity and the physical state of the dye. For the Neutral (NE) protolytic species the literature points out the zwitterionic NEZ tautomer only for fluorescein (X = H in Fig. 1) in the solid state, in aqueous solutions, and in water-rich mixtures.[8,17,18] However the amount of NEZ tautomer is negligible for halo-derivatives of fluorescein such as EOS and ERY.[16,19,20] The presence of halogen atoms in these dyes increase the acidity of the phenolic groups, preventing the existence of NEZ (structure in Fig. 1). In fact, the $pK_{a\text{-}OH}$ of EOS (2.02) and ERY (3.79) in water are much lower than the value reported for fluorescein (6.10).[15] Therefore in liquid solution for these halo-xanthenes only the tautomers NEL and NEQ are usually considered. On the other hand, the occurrence of the lactone NEL depends on the sp^3 hybridization of the carbon C9 (Fig. 1), with rupture of resonance on the chromophoric aromatic ring, leading to a dramatic decrease in the molar absorptivity (ε).[8,16,19] This lactone form prevails in organic non-protic solvents and with low dielectric constants,[16,21] while the quinoid NEQ structure is favored in polar solvents such as water.

[a] Department of Chemistry, Research Nucleus in Photodynamic System, State University of Maringa, Av. Colombo 5790, 87020-900, Maringa, PR, Brazil.
[b] Institute of Chemistry, Lab. of Photochemistry and Science Materials, Federal University of Uberlandia, Av. João Naves de Avila 2160, 38408-100, Uberlandia, MG, Brazil.
*Corresponding author: Tel.: +55-44-30113654. E-mail address: nhioka@uem.br
† Electronic Supplementary Information (ESI) available: Supplementary results of binding constant studies. See DOI: 10.1039/x0xx00000x

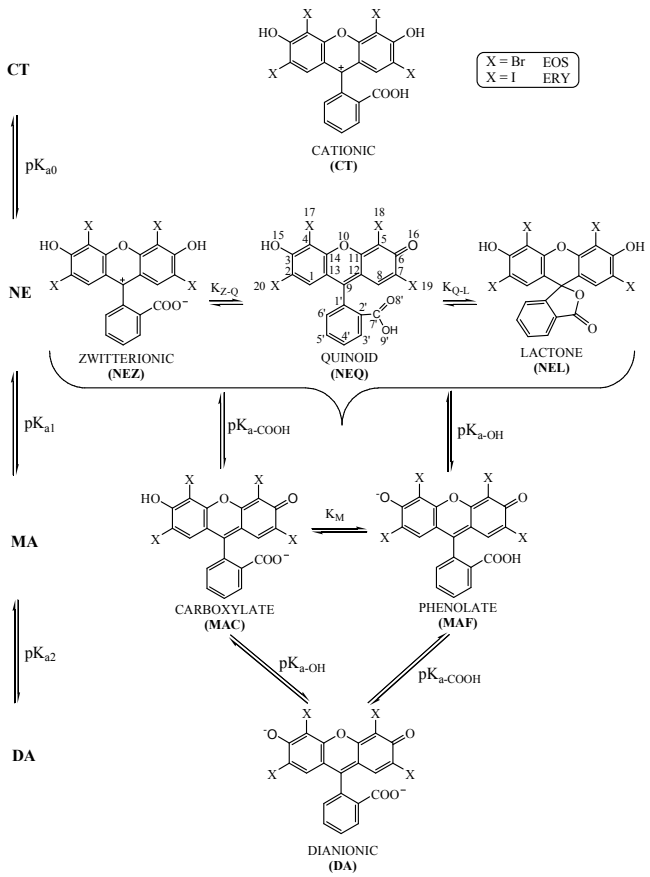

Fig. 1 Structures of EOS and ERY and theirs protolytic equilibrium between cationic CT, neutral NE, monoanionic MA and dianionic DA protolytic forms. Atom numeration for NEQ follows IUPAC norms.[15,16]

In a theoretical study involving monoanionic (MA) protolytic species of fluorescein in water and DMSO, Jang and co-workers discarded the lactone-type structure.[9] Therefore, two monoanionic tautomers are considered in the literature for ERY and EOS: the MAC and MAF structures that correspond to, respectively, the carboxylate bounded at the benzene ring and the phenolate group at the xanthene ring (structures in Fig. 1).

Moreover, usually carboxylic groups show higher acidity than the phenolic, *i.e.*, $pK_{a\text{-}COOH}<pK_{a\text{-}OH}$, being the negative charge of the basic form, better stabilized in the carboxylate than in the phenolate.[22] However this is not always true in halo-xanthenes, where the presence of four strong electron-withdrawing substituents in xanthene ring can promotes the pK_a inversion ($pK_{a\text{-}COOH}>pK_{a\text{-}OH}$).[15,16,23]

To investigate these complex acid-base systems and the participation of the tautomers on the equilibrium between the neutral and monoanionic protolytic species of halo-xanthenes, in the present study methyl ester derivatives of EOS and ERY were synthesized: the Eosin methyl ester (named as EOSMET) and Erythrosine methyl ester (named as ERYMET), Fig. 2.[15] These esters do not present the carboxylic group, facilitating the pK_a and the tautomeric analyses since the only possible equilibrium under this condition is MET-NE ⇌ MET-MA.[15] Using Multivariate Analysis techniques, it was reported that in aqueous solutions ERY (four iodine substituents) presented the usual $pK_{a\text{-}COOH}<pK_{a\text{-}OH}$, whereas EOS (four bromine substituents) showed the inversion $pK_{a\text{-}COOH}>pK_{a\text{-}OH}$. Actually, the challenge is to evaluate the role of each tautomer that allows their pK_a attribution for pK_{a1} (NE ⇌ MA) and pK_{a2} (MA ⇌ DA).

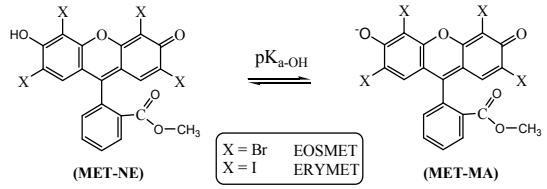

Fig. 2 Structures of esters derivatives EOSMET and ERYMET and the protolytic equilibrium between their neutral MET-NE and monoanionic MET-MA protolytic forms.[15]

Indeed the solvent can also promote the pK_a inversion, as reported by Mchedlov-Petrossyan for fluorescein in water/DMSO mixtures.[8] This effect was explained considering the shift of the tautomeric equilibrium of the neutral species at high percentages of DMSO, being justified by the prevalence of the NEL structure, demonstrated by the low absorbance of the neutral species (ε_{NEL}~ 0). This was also reported for 2,7-dichlorofluorescein in benzene/ethanol/water mixtures and in non-ionic micelles.[19]

Studies involving fluorescein tautomers were previously performed using Density Functional Theory (DFT) with the B3LYP hybrid functional, the basis set 6-31G, and the continuous solvation model of Poisson-Boltzmann with PCM (Polarizable Continuum Model) in water and DMSO.[9,24] Despite the tautomer mixtures in DMSO, this study suggested the MAF and NEL structures, as the main forms of the monoanionic and the neutral species. A computational study about the pK_a of fluorescein and its fluorine and chlorine derivatives showed good agreement with the experimental data and an increase of the acidity for halogenated compounds.[25] However, there still persist the need to understand the influence of bromine and iodine atoms on the properties of xanthene dyes.

In this work, studies were performed to elucidate the origin of pK_a inversion of ERY and EOS including the solvent dependence, as similarly pointed out to other xanthenes.[8,19] In this way, we try to clarify the extension of the tautomer's involvement for neutral and monoanionic species on the pK_a inversion using thermodynamic and spectrophotometric analysis by experimental data and molecular modeling in water, DMSO and their mixtures.

Materials and Methods

Experimental

All reagents of analytical grade were used as received. Solvents were previously purified. The Erythrosin B and Eosin Y were purchased from Vetec and theirs methyl esters were synthesized and characterized by NMR of ^1H and ^{13}C, and by FT-IR as reported.[5,15,26] The stock solutions of ERY and EOS were prepared in water, while ERYMET and EOSMET in DMSO. These stock solutions

were maintained frozen and in the dark for up to 2 weeks and were periodically standardized by UV-Vis electronic absorption measurement.

Experimental pK_a determination in water/DMSO mixtures

The pK_a of the dyes were determined in water/DMSO mixtures with the DMSO amount varying from 0 to 70% (v/v) using UV-Vis absorption spectrophotometry (Varian Cary-60). The measurements above 70% DMSO were not performed due to insolubility of the McIlvaine buffer ($[Na_2HPO_4]$ = [citric acid] = $7.5x10^{-3}$ mol L^{-1}). The experimental procedures and the calculation methodology by Multivariate Analysis techniques were similar to those previously utilized in pure water.[15] The pH measurements were performed using a Meterlab pHM 240 pH-meter equipped with a combined glass electrode. For water/DMSO mixtures the measurements were done against a saturated calomel electrode as reference. The ionic strength was controlled with NaCl 0.10 mol L^{-1}. The temperature was set at 30.0 °C in all experiments, and the dye concentration was maintained at $5.0x10^{-6}$ mol L^{-1}.

Calculation of the tautomeric equilibrium constants using experimental data

The calculation of the experimental tautomeric equilibrium constants (K_T) was done as reported in the literature.[8,16] Some approaches were assumed: (i) NEL is colorless ($\varepsilon_{NEL} = 0$) and (ii) the substituent connected to C2' (Fig. 1) caused no influence in the Visible absorption band, allowing to consider the spectral equivalence using the molar absorptivities $\varepsilon_{CT} = \varepsilon_{NEZ}$, $\varepsilon_{NEQ} = \varepsilon_{MAC}$ and $\varepsilon_{MAF} = \varepsilon_{DA}$ due the identical molecular structure of the chromophore ring.

For methyl esters, independent of the media, the neutral structure is necessarily the phenolic (named as MET-NE), where the chromophoric structure is similar to the tautomers MAC and NEQ of ERY and EOS, while the monoanionic form is a phenolate (named MET-MA), similar to MAF and DA (Fig. 2). Therefore it is proposed the following equivalence of absorptivities: $\varepsilon_{MET\text{-}NE} = \varepsilon_{NEQ} = \varepsilon_{MAC}$ and $\varepsilon_{MET\text{-}MA} = \varepsilon_{MAF} = \varepsilon_{DA}$. The presence of NEZ was discarded (molar fraction, $\chi_{NEZ} \sim 0$) as discussed before. Adopting these approaches for ERY and EOS, the calculation of the molar fraction χ of each neutral tautomer was performed using the equation $\varepsilon_{NE} = \varepsilon_{NEQ}.\chi_{NEQ} + \varepsilon_{NEL}.\chi_{NEL}$,[8,16]. However, if $\varepsilon_{NEL} = 0$, the resulting equation is

$$\varepsilon_{NE} = \varepsilon_{NEQ}.\chi_{NEQ} \quad \textbf{(1)}$$

where $\chi_{NEQ} + \chi_{NEL} = 1$.

For the monoanionic tautomer the molar fraction χ was calculated by a two variables two equation system, considering

$$\varepsilon_{MA} = \varepsilon_{MAC}.\chi_{MAC} + \varepsilon_{MAF}.\chi_{MAF} \quad \textbf{(2)}$$

where $\chi_{MAC} + \chi_{MAF} = 1$.

In Equations 1 and 2, ε_{NE} and ε_{MA} are the apparent molar absorptivities obtained from the experimental data of the total absorption intensity of mixed tautomers, respectively, for the neutral (NE) and monoanionic (MA) species. From the molar fraction of each structure the tautomeric equilibrium constant K_T for the neutral species ($K_{Q\text{-}L} = \chi_{NEL}/\chi_{NEQ}$) and for the monoanionic ($K_M = \chi_{MAF}/\chi_{MAC}$) was calculated.

Computational details

The structure optimizations were done initially for the NEQ of ERY in vacuum using the B3LYP hybrid functional[27] combined with the DGDZVP basis set.[28] This level of theory was chosen due the efficient results of molecular geometry and energy calculations allied to the low computational time, as previously reported.[28,29] All structural optimizations of ERY, ERYMET, EOS and EOSMET tautomers and protolytic forms were started from this optimized NEQ structure. The origin in this same cartesian plane ensures a geometric orientation similar to all species (Fig SI-1, Table SI-1 and Table SI-2 in Elec. Supp. Info.) and allows the comparison of dipole moments, even for the anionic species.[13]

Geometry optimizations and frequency calculations were also conducted using the B3LYP/6-311++G(d,p), M06-2X/DGDZVP and M06-2X/LANL2DZdp levels of theory. The iodine atom was described, using the *extrabasis* option, by the basis set LANL2DZdp ECP (DZP Double Zeta + Polarization + Diffuse ECP)[30] or by the basis set 6-311G(d,p)[31], both obtained from *Basis Set Exchange, version 1.2.2* (www.bse.pnl.gov). The DGDZVP basis set is also parameterized for iodine atoms and it was not necessary to include *extrabasis*. The same levels of theory were also used in the optimizations of these species solvated in water and DMSO using the IEF-PCM[32] solvation model. All the optimized structures were characterized as real minima since in the frequency calculations imaginary frequencies were not found. The Standard Gibbs Free Energy of Solvation ($\Delta G°_{sol}$) was estimated by single point calculations using IEF-PCM and SMD solvation models with UFF, Pauling and Coulomb (only for SMD) atomic radii sets.[33,34,35] Analyses of NBO (Natural Bonding Orbital) were done with B3LYP/DGDZVP in vacuum and using SMD-Coulomb solvation model. Delocalization energies were calculated using the natural bond orbital analysis method (NBO 3.1) by zeroing all orbitalar interactions using the keywords *pop=nbodel* and *nostar*.

Implicit-explicit calculations were also performed with the neutral and monoanionic tautomers of ERY and EOS, adding 3x water molecules: at the side of each O15, O16 and O9' oxygens (Fig.1); or 6x water molecules: at the side of each O15 and O16 oxygens and 4x at side of the carboxylic group. For this the B3LYP/DGDZVP level of theory and IEF-PCM/UFF solvation model were used to optimization and frequency calculations. After that, the SMD/Coulomb solvation model in the same level of theory was used to perform single point calculations with the optimized structures. For the calculations of tautomeric equilibria (K_T) of neutral forms, the electronic energy (E_0) was corrected considering the Basis Set Superposition Error[36] of the 6x water molecules with the xanthene dyes, adding the solute-solvent interaction energy (ΔE_{int}) to the solute energy. UV-Vis absorption spectra were simulated using the TD-DFT approach at the B3LYP/DGDZVP, B3LYP/6-311++G(d,p), CAM-B3LYP/DGDZVP, CAM-B3LYP/6-311++G(d,p) and M06-2X/DGDZVP levels of theory along with the solvation models SMD and IEF-PCM.

The UFF, Pauling and SMD-Coulomb radii sets were tested on DA, MET-NE, and MET-MA of ERY and EOS in water. The closest agreement with the experimental maximum wavelength, λ_{max}, was achieved using B3LYP/6-311++G(d,p) along with the SMD-Coulomb solvation model. In this way, this combination was used throughout all the remaining calculations in water and DMSO. All calculations were carried using the Gaussian 09 software package, revision A.01.[37] The schematic illustrations of Figs. 1, 2, 7 and 10 were generated using the CS ChemDraw Ultra® software.[38]

The tautomeric equilibrium by chemical-computational treatments

The Standard Gibbs Free Energy of Reaction (ΔG_r^o) involves the electronic energy (E_o) plus the thermal correction for the free energy (G_{corr}) obtained from a frequency calculation.[39] The values of ΔG_r^o for the equilibria NEQ ⇌ NEL ($\Delta G_{r(Q-L)}^o$) and MAC ⇌ MAF ($\Delta G_{r(M)}^o$) were evaluated in water and DMSO at 298.15 K using Equation 3,

$$\Delta G_r^o = \sum(E_0 + G_{corr})_{prod} - \sum(E_0 + G_{corr})_{reag} \quad \textbf{(3)}$$

For the solvation of each specie the IEF-PCM and SMD models were tested varying the radii set of UFF, Pauling and SMD-Coulomb in Single Point calculations aiming to improve the electronic energy (E_o) results. The G_{corr} was obtained with IEF-PCM/UFF trough frequencies calculations. The E_o and G_{corr}, applied to Equation 3 for each specific equilibrium, furnished $\Delta G_{r(Q-L)}^o$ and$\Delta G_{r(M)}^o$. From these $\Delta G_{r(T)}^o$, the tautomerization equilibrium constants $K_{Q\text{-}L}$ and K_M were determined by Equation 4, where R is 1.987x10^{-3} kcal/mol K.[40-42] This treatment also permitted to verify the role of NEZ in the equilibrium with NEQ and NEL,

$$K_T = e^{-(\Delta G_r^o)/RT} \quad \textbf{(4)}$$

pK$_a$ calculation using computational methodology

The pK$_a$ calculation of the protolytic processes was performed using Equation 5, which considers the variation of the Standard Gibbs Free Energy of deprotonation of an acid (HA) in water (ΔG_{aq}^o) or DMSO (where ΔG_{aq}^o is replaced by ΔG_{dmso}^o), obtained from the thermodynamic cycle illustrated in Supp. Info., Scheme SI-1.[43,44] The Standard Gibbs Free Energy (G^o) in gas phase of the protonated (HA_{gas}) and deprotoned (A^-_{gas}) forms were obtained from frequency calculations performed at each level of theory evaluated. The study followed a methodology described in the literature,[43,45] using optimized structures in water or DMSO (IEF-PCM/UFF) to perform Single Point calculations, obtaining the ΔG_{sol}^o values for HA and A$^-$. In these calculations, the solvation models IEF-PCM and SMD were tested together with the radii sets UFF, Pauling and SMD-Coulomb.

$$pK_a = \frac{\Delta G^\circ_{aq}}{RT \ln 10} \quad \textbf{(5)}$$

The resolution of the thermodynamic cycle in water results in the following expression for ΔG_{aq}^o (Equation 6), that is included in Equation 5,

$$\Delta G^\circ_{aq} = G^\circ_{gas}(A^-) + G^\circ_{gas}(H^+) - G^\circ_{gas}(HA) + RT\ln(24.46) + \Delta G^\circ_{sol}(A^-) + \Delta G^\circ_{sol}(H^+) - \Delta G^\circ_{sol}(HA) \quad \textbf{(6)}$$

Using values tabulated for H$^+$, $G_{gas}^o(H^+)$= -6.28 kcal/mol and $\Delta G_{sol}^o(H^+)$= -265.9 kcal/mol[44-50] at 298.15 K, R = 1.987 cal/K mol, T = 298.15 K and corrected for ΔG_{gas}^o*(1 atm)* to ΔG_{gas}^o*(1 mol L^{-1})* with the factor RTln(24.46),[51] the Equation 6 reduces to Equation 7,

$$\Delta G^\circ_{aq} = G^\circ_{gas}(A^-) - G^\circ_{gas}(HA) + \Delta G^\circ_{sol}(A^-) - \Delta G^\circ_{sol}(HA) - 270.3 \quad \textbf{(7)}$$

After the correction of ΔG_{sol}^o for the transfer of H$^+$ from water to DMSO, at 298.15 K, in agreement to IUPAC norms[52] the value of $\Delta G_{sol}^o(H^+)$=-268.63 kcal/mol could be estimated. This value was introduced in Equation 6 resulting in ΔG_{dmso}^o (Equation 8). After that, ΔG°_{DMSO} was introduced in Equation 5 for the pK$_a$ calculus,

$$\Delta G^\circ_{DMSO} = G^\circ_{gas}(A^-) - G^\circ_{gas}(HA) + \Delta G^\circ_{sol}(A^-) - \Delta G^\circ_{sol}(HA) - 273.0 \quad \textbf{(8)}$$

It was also possible to estimate the pK$_a$ in gas phase from ΔG_{gas}^o,

$$\Delta G^\circ_{gas} = G^\circ_{gas}(A^-) - G^\circ_{gas}(HA) - 6.28 \quad \textbf{(9)}$$

Two other thermodynamic cycles were tested, showed in Elec. Supp. Info.. One of them is the proton exchange method (Scheme SI-2), including a reference acid compound (HRef),[44] obtaining the pK$_a$ results with Equation 10 and Equation 11. The HRef used was ERYMET and EOSMET for pK$_a$ calculations of ERY and EOS, respectively.

$$pK_a = \frac{\Delta G^o{}_{aq}}{RT\ ln10} + pKa(HRef) \quad \textbf{(10)}$$

$$\Delta G^o{}_{aq} = G_{gas}(HRef) - G_{gas}(Ref^-) + G_{gas}(A^-) - G_{gas}(HA) + RTln24.46 + \Delta G_{sol}(HRef) - \Delta G_{sol}(Ref^-) + \Delta G_{sol}(A^-) - \Delta G_{sol}(HA) \quad \textbf{(11)}$$

In the second cycle the neutral and monoanionic species were optimized with 3x explicit water molecules (Scheme SI-3, Eq SI-1 and Eq SI-2).[46-50]

Results and discussion

Experimental values of pK$_a$ in water/DMSO mixtures

The electronic absorption spectra of ERY, ERYMET, EOS and EOSMET as representative systems in mixtures of water/DMSO at 70% DMSO shows that the intensity of the main peak varies as function of pH (Fig. 3).

The profile of spectral changes for ERY and EOS (Figs 4A and 4C) in the DMSO-rich medium (70% of DMSO) presents a two-phase variation: an expressive increase (1), followed by a hypsochromic shift in higher pH values (2). These two steps correspond to the equilibria associated with pK$_{a1}$ and pK$_{a2}$. These variations are significantly different from the spectra obtained in pure water, as reported earlier,[15] which show that the dissociation constants are highly sensitive to the local dielectric constant. On the other hand, the esters, which possess just one acid-base unit, pK$_{a\text{-}OH}$, only show the peak growth, a similar profile observed in water.[15]

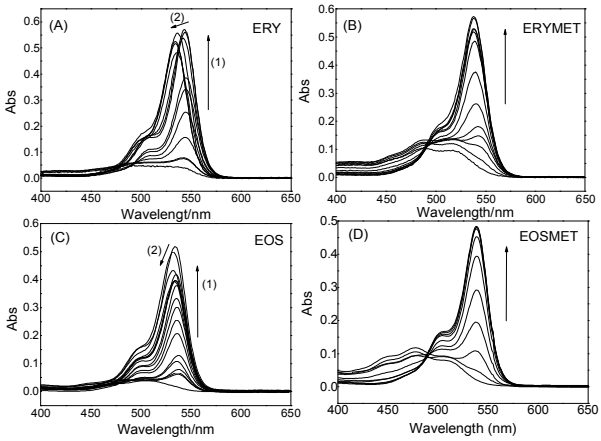

Fig. 3 Sequence of the electronic absorption spectra for: (A) ERY; (B) ERYMET; (C) EOS and (D) EOSMET in water/DMSO mixtures at 70% (v/v) DMSO. pH range of 0 to 8 in buffer or HCl solutions. Dyes 5.00x10^{-6} mol L^{-1}, NaCl 0.10 mol L^{-1} and 30.0 °C. The arrows point out the variation as the pH increases.

Despite these differences, the profile of the absorption intensity at the λ_{max} against pH was similar for ERY and EOS compared to their respective methyl ester derivatives. All xanthenes investigated have the phenolic group connected to the xanthene ring, which belongs to the chromophore region of the molecule. However for the non-esters the presence of the carboxylic substituent connected to the benzene ring exhibits an inefficient resonance conjugation with the chromophoric xanthene group due to the orthogonality between these two molecular moieties. This implies that the configurations, carboxylic or carboxylate, exert only a small influence on the absorption spectra while the phenolic-phenolate equilibrium is the main responsible for the changes.[53]

Indeed the fact that for ERYMET and EOSMET $pK_a = pK_{a\text{-}OH}$, helps the assignment of the pK_a value of each corresponding acid-base group for ERY and EOS in water by comparison.[15] The same approach in these study was applied for water/DMSO mixtures: $pK_{a,ERYMET} \sim pK_{a\text{-}OH,ERY}$ and $pK_{a,EOSMET} \sim pK_{a\text{-}OH,EOS}$. These comparisons and the spectral profile as a function of the pH permitted the pK_a attributions.[15]

The mathematical strategy applied to the absorbance spectra as a function of pH was the Henderson-Hasselbalch equation[15] that resulted in the values listed in Table 1 for water/DMSO mixtures. As observed in water ERY shows $pK_{a\text{-}COOH} < pK_{a\text{-}OH}$ as previously reported, while for EOS $pK_{a\text{-}COOH} > pK_{a\text{-}OH}$.[15]

In addition, Table 2 shows the "apparent" molar absorptivity at the wavelength of the most prominent absorption band (λ_{max}) of each protolytic species, which for the neutral and monoanionic species corresponds to a mixture of tautomers. These data were obtained from Matrix-K method[54] combined to experimental spectrophotometric measurements.

For clarity reasons the data shown in Table 1 for ERY and EOS were depicted from a plot of pK_a *versus* DMSO percentage (Fig. 4). All pK_a values increase as the fraction of DMSO increases, showing a linear profile previously observed for several organic acids at different solvent mixtures.[21,55,56] The importance of the water molecules in the stabilization of charged structures is well-known. The absence of water in the solvent usually leads the charge separation to an energetically unfavorable condition, leading to low acidity (that corresponds to pK_a increases as the amount of DMSO increases).[8,19]

Table 1 Values of pK_a for the xanthenes investigated in different water/DMSO mixtures of [dye]= 5.0x10^{-6} mol L^{-1} and [NaCl]= 0.10 mol L^{-1}, at 30.0 °C. The pK_a values are expressed as average value ± standard deviation, resulting from the curve fitting using the Henderson-Hasselbalch equation.

DMSO % (v/v)		0[a]	20	40	60	70
ERY	$pK_{a\text{-}OH}$	3.79 ± 0.08	3.97 ± 0.02	4.09 ± 0.21	4.41± 0.05	4.58 ± 0.10
	$pK_{a\text{-}COOH}$	2.35 ± 0.09	3.39 ± 0.04	4.62 ± 0.17	5.55 ± 0.08	5.93 ± 0.08
ERYMET	$pK_{a\text{-}OH}$	3.74 ± 0.07	3.89 ± 0.04	3.99 ± 0.05	4.51 ± 0.03	4.64 ± 0.03
EOS	$pK_{a\text{-}OH}$	2.02 ± 0.05	2.24 ± 0.08	*	*	2.04 ± 0.05
	$pK_{a\text{-}COOH}$	3.80 ± 0.06	5.03 ± 0.05	*	*	7.07 ± 0.09
EOSMET	$pK_{a\text{-}OH}$	2.11 ± 0.03	2.05 ± 0.05	*	*	2.36 ± 0.07

[a]from Batistela *et al.*(2011)[15] *not measured because the small variation in the range of 20 to 70 % DMSO.

Table 2 Apparent molar absorptivities (**ε**) of protolytic species NE, MA and DA at the maximum absorption band wavelength (λ_{max}) in water/DMSO, obtained with Matrix-K method.

		λ_{max} (nm); ε (10^3 L mol^{-1} cm^{-1})				
[DMSO] % (v/v)		0	20	40	60	70
ERY	NE	491; 15.6	493; 15.8	492; 10.5	490; 5.3	494; 3.2
	MA	529; 41.2	533; 31.7	535; 84.9	540; 93.6	543; 95.6
	DA	527; 96.5 [a]	527; 99.0	530; 93.3	531; 98.5	532; 100.5
ERYMET	NE	491; 19.8	492; 20.1	494; 18.8	494; 19.3	493; 20.6
	MA	527; 92.8 [a]	531; 95.6	535; 97.6	539; 99.7	541; 101.4
EOS	NE	470; 7.5 [a]	470; 7.4	*	*	470; 8.3
	MA	519; 51.7 [a]	519; 48.9	*	*	519; 53.7
	DA	515; 96.7 [a]	517; 97.4	*	*	517; 95.7
EOSMET	NE	470; 16.8	470; 13.1	*	*	470; 16.2
	MA	517; 97.2 [a]	517; 96.4	*	*	517; 113.4

[a] From Batistela *et al.*(2011)[15] *not measured.

RSC Advances

ARTICLE

For NE and MA of the non-ester and ester xanthenes, the apparent molar absorptivity (Table 2) depends on the amount of DMSO. This is related to differences in the molecular solvation between the involved tautomers for each protolytic species.

However as observed, the increase of pK_a of the carboxylic group for both dyes is pronounced, while for the phenolic group of ERY it is much less significant, remaining almost unchanged for the phenolic group of EOS. In fact, the influence of water for the carboxylic-carboxylate equilibrium ($pK_{a\text{-}COOH}$), especially for the carboxylate group, is very expressive in ERY. However, it is not relevant for the phenolic-phenolate ($pK_{a\text{-}OH}$) equilibrium for ERY and EOS. The reason is that the charge on the phenolate is naturally delocalized over the xanthene ring. Therefore the relevance of solvation in phenolic-phenolate equilibrium should be minimal. This explains the high influence of water/DMSO composition on pK_a: small for $pK_{a\text{-}OH}$ and high for $pK_{a\text{-}COOH}$. However this analysis must be much more complex due the involvement of the tautomers. For NE (NEQ, NEL and NEZ) and MA (MAC and MAF), which exhibits strong effect on the pK_a, the solvation effects influences the tautomeric equilibrium.

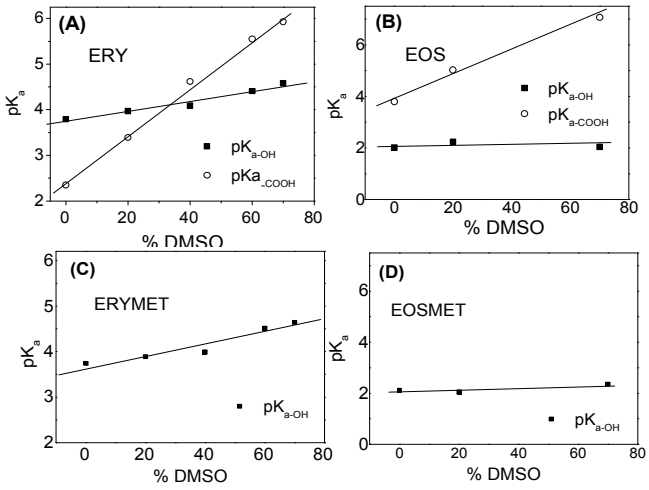

Fig. 4 pK_a values *versus* DMSO percentage (v/v) in water for: (A) ERY and (B) EOS (C) ERYMET and (D) EOSMET. Dyes 5.00×10^{-6} mol L^{-1}, NaCl 0.10 mol L^{-1} and 30.0 °C.

As result for ERY at 0 to 35% of DMSO (v/v), Fig. 4A shows $pK_{a\text{-}OH} > pK_{a\text{-}COOH}$, where $pK_{a\text{-}OH} = pK_{a2}$ implies in a predominance of the MAC form for the monoanionic species, in equilibrium with DA. For situations in which the fraction of DMSO is higher than 35% in the mixture, a pK_a inversion is verified for ERY (Fig. 4A), which leads to $pK_{a\text{-}COOH}=pK_{a2}$, involving the equilibrium between MAF and DA (Fig. 1). This occurs because the equilibrium of the monoanionic species is displaced (MAC → MAF) as the dielectric constant of the solvent is reduced (as the presence of DMSO increases). Similar results were observed for other xanthene dyes in water mixtures with organic solvents.[19,53,57] On the other hand, EOS shows $pK_{a\text{-}OH}<pK_{a\text{-}COOH}$ in all samples independent of DMSO presence (Fig. 4B) due the influence of the four bromine substituents as already mentioned, which theoretically favors the stabilization of the monoanionic MAF tautomer, leading to $pK_{a2} = pK_{a\text{-}COOH}$ and consequently $pK_{a1} = pK_{a\text{-}OH}$. However, the involvement of the monoanionic tautomer form of MAC or MAF and the neutral tautomers NEQ or NEL (and maybe NEZ) on pK_{a1}, is not so easy to be defined for ERY and EOS. Therefore a quantitative analysis was performed later.

In Fig. 4 it is included the pK_a values for the methyl esters. As demonstrated the profile of the $pK_{a\text{-}OH}$ of ERY and EOS as a function of DMSO percentage is identical to the profile observed for ERYMET (Fig. 4C) and EOSMET (Fig. 4D), respectively, which reinforces the correctness of the pK_a attribution.

Structural description and computational analysis of stability

The application of the two selected levels of theory, B3LYP/DGDZVP and B3LYP/6-311++G(d,p), resulted in structures with identical conformation with dihedral angles in agreement with the literature.[9,13,58,59] For all optimized structures, except for NEL, the averaged dihedral angle between the xanthene and the benzene rings (C13-C9-C1'-C2', atom numeration in Fig. 1) was about 91°, while between the carboxylic group and the benzene ring (C1'-C2'-C7'-O8') it was of only 1°. The structures of NEQ and NEL of ERY and the dihedral angles were included in the Supp. Info., Fig. SI-1 and Table SI-1. For NEL the lactone ring has the benzene ring orientation shifted, leading the dihedral angle C13-C9-C1'-C2' to 115°.[13,59] The Cartesian planes of each optimized species of ERY, ERYMET, EOS and EOSMET are also included in the Supp. Info., Table SI-1.

The Molecular Electrostatic Potential maps (MEP) for neutral NEQ and NEL and the monoanionic MAC and MAF in water are depicted in Fig. 5, with a half of the dipole moment vector. The dipole moment of each form in water, DMSO and vacuum obtained using B3LYP/6-311++G(d,p) and SMD-Coulomb is listed in Table SI-3 in Supp. Info.

As illustrated in Fig. 5 the MEP of NEQ shows regions with higher negative density (strong red color) than NEL, which means that NEQ presents high polarity while NEL exhibits a more homogeneous charge distribution, which agrees with the difference observed for the dipole moments ($\mu_{NEQ}>\mu_{NEL}$) in water: for ERY, μ_{NEQ}=19.59 and μ_{NEL}=9.46 debye; for EOS, μ_{NEQ}=18.47 and μ_{NEL}=9.02 debye. These results confirm and justify the higher stabilization of NEL in environments with low dielectric constants such as in DMSO, and the opposite effect for NEQ in water.

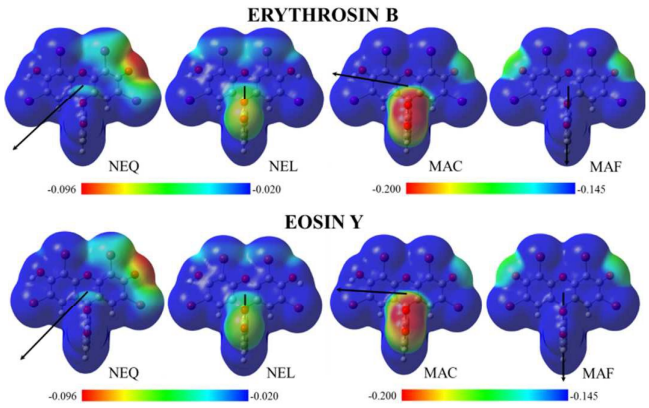

Fig. 5 Molecular Electrostatic Potential maps (MEP) for tautomers of ERY and EOS obtained from B3LYP/DGDZVP and SMD-Coulomb in water, keeping the isovalue of the density at 0.0004 e/Å^3. The arrows represent a half of the values of the dipole moment vector (μ) pointed to a positive region.

The MEP obtained for MAC shows a high negative charge density on the carboxylic group while MAF exhibits a homogeneous charge distribution (Fig. 5), suggesting that $\mu_{MAC} > \mu_{MAF}$ which is confirmed by the data in water: for ERY μ_{MAC}=20.82 and μ_{MAF}=15.85 debye; for EOS μ_{MAC}=19.46 and μ_{MAF}=17.40 debye. This effect in water is much more evident than in DMSO or vacuum (Table SI-3).

These data explain the higher stabilization of NEQ and MAC in water and NEL and MAF in solvents with low dielectric constants, as previously observed.[19,20,57] The carboxylate group of MAC exerts strong interactions with water by dipole-dipole affinity and hydrogen bonding, while for MAF its homogeneous charge distribution leads to low charge density in the phenolate group, resulting in weak interactions with water.[22,60]

Experimental tautomeric equilibrium constants and its influence on pK$_a$

For molar fraction (χ) calculations, the absorption intensities were taken at the maxima wavelength (λ_{max}) instead of one analytical wavelength due to solvatochromic effects (Table 2). The results of χ for each tautomer and the tautomeric equilibrium constants ($K_{Q\text{-}L}$ and K_M) are listed in Table 3.

The results in Table 2 and 3 permit the quantitative analysis:

ERY/water: For DMSO range (0 - 35%), the molar absorptivity values ε (Table 2) of the neutral form of ERY are only ~27% lower than the ERYMET (MET-NE), suggesting small participation of the colorless lactone NEL tautomer and consequent prevalence of the quinoid NEQ for ERY. For monoanionic species in water, the absorptivity (Table 2) of ERY is less than half of the phenolate-type structure MET-MA of ERYMET. Consequently, there is a significant presence of both MAF and MAC. In fact, results in Table 3 show that water favors not only the neutral NEQ form ($K_{Q\text{-}L}$<1 with χ_{NEQ}= 0.79 in water) but also the monoanionic MAC (K_M<1 with χ_{MAC}= 0.71 in water). Both NEQ and MAC tautomers (carboxylate-types) show higher molecular polarity than, respectively, NEL and MAF (phenolate-type structures), as demonstrated by MEPs and dipole computational results. Therefore water molecules preferentially stabilize the formers by dipole interactions allied to hydrogen bonds rather than phenolic-phenolate compounds.[22,60] Thus, for ERY in water, pK_{a1} is proposed NEQ ⇌ MAC, and for pK_{a2} MAC ⇌ DA, with $pK_{a\text{-}COOH} < pK_{a\text{-}OH}$ (Fig. 1).

ERY/DMSO: As observed at above 35% of DMSO for ERY, data in Table 2 show an accentuated absorptivity decrease for the neutral form and a substantial increase for the monoanionic form. The low ε values for the neutral species point out the equilibrium displacement in DMSO to NEL (colorless). Indeed the ε values at ~540 nm of the monoanionic form of ERY exhibit similarity with ERYMET (MET-MA) that reinforce the MAF prevalence for ERY above 35% of DMSO (both MET-MA and MAF are phenolate-type structure). Actually, Table 3 data confirm that DMSO favors the NEL ($K_{Q\text{-}L}$>1 with χ_{NEL}= 0.84 at 70% DMSO) and the MAF (K_M>1 with χ_{MAF}= 0.93 at 70% DMSO) forms, both less polar than NEQ and MAC (carboxylate-type structures). This result permits to associate the equilibria NEL ⇌ MAF as pK_{a1} and MAF ⇌ DA as pK_{a2}, that correspond to $pK_{a\text{-}OH} < pK_{a\text{-}COOH}$, for ERY in DMSO-rich media. However an unsolved problem remained: Would it be possible the direct transformation of NEL in MAF? This problem is discussed below.

EOS/water-DMSO: In Table 3 the value $K_{Q\text{-}L}$= 1.24 found in water at 30°C agrees with the value at 25°C reported in the literature (1.3).[11] Therefore in water, beside NEL (χ_{NEL}= 0.55), there is a significant amount of co-existing NEQ (χ_{NEQ}= 0.45). Despite this, for EOS where $pK_{a\text{-}OH} < pK_{a\text{-}COOH}$, the same proposition as ERY in DMSO would be expected NEL ⇌ MAF (pK_{a1}) and MAF ⇌ DA (pK_{a2}). The MAF participation in pK_{a2} is fully justified by the $pK_{a2} = pK_{a\text{-}COOH}$ based on structural analysis of MAF ⇌ DA equilibrium (structures in Fig. 1).

However, while the monoanionic form of ERY exhibited similar absorptivity to ERYMET as previously mentioned, for EOS the monoanionic form presents absorptivity around 50% lower than the value of the monoanionic EOSMET (MET-MA, phenolate-type), which presents a structure similar to MAF.

Table 3 Molar fractions (χ) of tautomers NEL – NEQ (neutral species) and MAC – MAF (monoanionic species) of ERY and EOS and their tautomeric equilibrium constants. Experimental results in water-DMSO mixtures at 30.0 ºC.

	ERY					EOS		
DMSO % (v/v)	**0**	**20**	**40**	**60**	**70**	**0**	**20**	**70**
χ_{NEQ}	0.79	0.79	0.56	0.28	0.16	0.45	0.56	0.51
χ_{NEL}	0.21	0.21	0.44	0.72	0.84	0.55	0.44	0.49
$K_{Q-L} = \chi_{NEL}/\chi_{NEQ}$	0.27	0.27	0.79	2.64	5.51	1.24	0.77	0.96
χ_{MAF}	0.29	0.15	0.84	0.84	0.93	0.43	0.43	0.39
χ_{MAC}	0.71	0.85	0.16	0.16	0.07	0.57	0.57	0.61
$K_M = \chi_{MAF}/\chi_{MAC}$	0.41	0.18	5.21	5.17	12.89	0.75	0.75	0.63

Thus, this result indicates not negligible involvement of MAC in pK_{a1}. In fact, K_M=0.75 from Table 3 implies in MAC preference (χ_{MAC}= 0.57) with still high amounts of MAF (χ_{MAF}= 0.43).

Anyway, taking the experimental preferential structures, the resulting equilibrium for pK_{a1} is NEL ⇌ MAC, while for pK_{a2} the structural analysis pointed out unequivocally MAF ⇌ DA, which is not consistent for a pH region between pK_{a1} and pK_{a2}. Similar as in water, the same pK_a inversion is observed for EOS in water/DMSO mixtures where the relative amount of each tautomer underwent small changes (χ_{NEL}= 0.49 and χ_{NEQ}= 0.51; χ_{MAC}= 0.61 and χ_{MAF}= 0.39 in 70% DMSO). However, it is possible to consider NEQ ⇌ MAF as pK_{a1}, which implies in a phenolic-phenolate equilibrium once the amount of NEQ is considerably higher in both water and DMSO.

NEL → MAF conversion: NEL prevails for ERY in DMSO-rich media (Table 3) and presents high molar fraction for EOS in water and in DMSO ($\chi_{NEL} \sim \chi_{NEQ}$, Table 4). However, it is impossible to transform NEL to MAF directly, which is a problem for pK_a inversion: pK_{a2} should be equal to $pK_{a\text{-}COOH}$ involving necessarily MAF. For this process two hypotheses can be presented:

(a) NEL → MAF Problem: The NEL form can be converted to NEQ, which is an unstable intermediate in this situation, that is immediately consumed by deprotonation of O15 resulting in MAF, {NEQ →→ MAF} with $pK_{a1} = pK_{a\text{-}OH}$. In principle the NEL → NEQ conversion seems to be inconsistent in solvents with low dielectric constant such as DMSO. However independent of the prevalence of NEL or NEQ the equilibrium NEL ⇌ NEQ occurs and the protolytic equilibrium is NEQ ⇌ MAF with $pK_{a1}=pK_{a\text{-}OH}$ (where for ERY in 70% of DMSO, χ_{MAF}= 0.93 while $\chi_{MAF} \leq \chi_{MAC}$ for EOS in the range of 0 to 70% of DMSO). Therefore the protolytic equilibrium related to pK_{a2} involves MAF (with DA, $pK_{a2}=pK_{a\text{-}COOH}$).

(b) NEL undergoes the simultaneous deprotonation of O16 and the ring rupture of the lactone due to resonance reorganization, leading to MAC as an unstable intermediate in DMSO, which is consumed by hydrogen transfer from O15 to O9', resulting in MAF {NEL → MAC (unstable in DMSO) →→ MAF}. However the step MAC →→ MAF should be very fast since it occurs by hydrogen transfer, which does not explain the χ_{MAC}= 0.57 higher than the MAF in EOS (Table 4). This second hypothesis is not convincing.

Indeed, despite the slight preference to MAC in water, the K_M for EOS (0.75) is higher than the value for ERY (0.41), which means that the amount of MAF for EOS (χ_{MAF}= 0.43) is higher than MAF for ERY (χ_{MAF}= 0.29). This difference in MAF stabilization seems to favor the pK_a inversion for EOS even in water. In summary it is not only the NEL prevalence that commands the pK_a inversion but also the tautomeric equilibrium between MAC and MAF.

The pK_a inversion is consistent with the action of organic solvents on phenolic and carboxylic groups, where the inversion is associated to the solvation capability of these groups against their respective conjugated bases.[22,60] Similar effects were observed in other studies involving xanthene dyes in mixtures of water/organic solvents.[8,19,20,53,57]

Evaluation of the tautomeric equilibrium using computational methods of electronic structure

During our previous computational studies on structure optimization in vacuum and water, using only the IEF-PCM continuous solvation method, the NEZ form always converged to the lactone NEL. To investigate computationally the NEZ structure, the following strategies were applied: (i) the length between the atoms O8' and C9 (Fig. 1) was fixed as 2.5 Å (averaged value for all other structures), which prevents the cyclization to NEL; (ii) the addiction of 3x or 6x explicit water molecules within the IEF-PCM model, however without fixing the O8'–C9 length.

Given the results of the optimized structures NEZ, NEQ and NEL, the tautomeric equilibrium NEZ ⇌ NEQ and NEZ ⇌ NEL was firstly analyzed. The calculation of the tautomeric equilibria in water and DMSO using only IEF-PCM/UFF and SMD/Coulomb continuous solvation models with B3LYP/6-311++G(d,p) resulted in tautomeric equilibrium constants (K_T) ranging from $5.19x10^7$ in water to $5.0x10^9$ in DMSO, favoring the formation of NEQ and NEL. Including 3x explicit water molecules the NEZ structure also converged to NEL during the optimization without fixing the O8'-C9 length. However with 6x explicit water molecules the NEZ form was optimized as a real minimum of energy. Thus, the NEL and NEQ tautomers were optimized with 6x explicit water molecules and, after single points calculations at B3LYP/6-311++G(d,p) with SMD/Coulomb, the following K_T results were obtained: To ERY the NEZ ⇌ NEQ ($K_{Z\text{-}Q}$= $3.93x10^4$) and NEZ ⇌ NEL ($K_{Z\text{-}L}$= $1.76x10^3$) confirming a small participation of NEZ at the neutral equilibria. The same behavior could be seen with EOS, with NEZ ⇌ NEQ ($K_{Z\text{-}Q}$= $3.70x10^5$) and NEZ ⇌ NEL ($K_{Z\text{-}L}$= $3.47x10^3$). These theoretical results are in agreement with the literature, that affirms the absence of expressive amounts of NEZ in these solutions.[8,16,21,25,61] The quantitative comparison of the equilibrium constants *via* computational method with the experimental values is impracticable due the differences in temperature and dependence with the used theory level, which give considerable errors, especially for bulky substituents such as iodine.[44,62] Despite this, the results permit to evaluate the tendencies of the equilibrium by comparison between the tautomers, where errors should be minimized by compensation.

The data of tautomerization constant for ERY in water for the most relevant neutral forms (NEQ ⇌ NEL) and monoanionic (MAC ⇌ MAF) species, calculated using the functional B3LYP and M06-2X are shown in Table SI-4, Elec. Supp. Info. The M06-2X/DGDZVP and M06/LAN2DZ(d,p) levels of theory combined with IEF-PCM or SMD solvation methods, simulating the solvation in water, in combination with the atomic radii sets UFF, Pauling or SMD-Coulomb furnished a $K_{Q\text{-}L}$ >>1 for the neutral species, and K_M >>1 for the monoanionic. These values are quite different of the experimental ones ($K_{Q\text{-}L}$= 0.27 and K_M= 0.41, Table 4).

The results using the B3LYP hybrid functional for NEQ ⇌ NEL and MAC ⇌ MAF in Table 4 (short) and Table SI-4 (complete) gave a better description of the qualitative behavior of the tautomeric equilibria, being closer to the experimental ones.

ERY/water: For ERY in water, using B3LYP/DGDZVP and B3LYP/6-311++G(d,p) with all solvent models and radii sets, Table 4, it was observed the predominance of NEQ ($K_{Q\text{-}L}$ < 1), also with 6x explicit water molecules ($K_{Q\text{-}L}$= 0.045), which agrees with the experimental finds (χ_{NEQ}= 0.79, Table 3). The use of the basis set DGDZVP with the IEF-PCM/UFF ($K_{Q\text{-}L}$= 0.22) resulted in values close to the experimental ones ($K_{Q\text{-}L,exp}$= 0.27). However this methodology for the anionic species in water led to very high K_M values (magnitude of 10^4) suggesting a much greater stability to MAF than for MAC in disagreement with the experimental finding, where χ_{MAC} is 0.71 (Table 3). Possibly this disagreement is related to basis set limitations, once it is not possible to add diffuse function to iodine or even other atoms using DGDZVP.

The addition of diffuse functions would permit a better description by the inclusion of increased Gaussian functions in the valence shell.[63,64] For example, the use of the basis set 6-311++G(d,p) improved somewhat the agreement between the predicted K_M and $K_{Q\text{-}L}$ and the experimental values (Table 4). Iodine atoms, however, does not receive diffuse functions when this triple-zeta basis is added using the *extrabasis* keyword. This is one possible reason why K_M and $K_{Q\text{-}L}$ still remain far from experimental results.

ERY/DMSO: For the neutral form of ERY in DMSO, only DGDZVP with SMD/Coulomb properly described the experimental equilibrium constant NEQ ⇌ NEL, $K_{Q\text{-}L}$>1 that correctly means NEL prevalence. For anionic species both levels of theory, B3LYP/DGDZVP and B3LYP/6-311++G(d,p), properly described the experimental findings with solvation models, whose high values of K_M confirm MAF as the main tautomer in DMSO. Thus, both theoretical levels pointed out for the involvement of the NEL and MAF when pK_a inversion occurs, as in experiments involving ERY at high proportions of DMSO.

EOS/water-DMSO: For EOS in water (Table 4), only the DGDZVP basis set with the IEF-PCM/UFF described the equilibrium of the neutral species with a small shift to NEL, with $K_{Q\text{-}L}$ quite close to experimental data. SMD/Coulomb pointed out NEQ as favored, even with 6x water molecules ($K_{Q\text{-}L}$=0.0094) agreeing with our previous proposition.[15] However, this does not agree with our actual experimental findings (χ_{NEQ}= 0.45 in water, Table 3).

The NEL participation reinforces the pre-equilibrium NEQ ⇌ NEL shifted to NEQ, where this tautomer is immediately consumed in the equilibrium with MAF, leading to pK_{a1}=$pK_{a\text{-}OH}$ with pK_a inversion (*Hypothesis for NEL → MAF*). Anyway, it is clear that for monoanionic species the computational calculation (Table 5) points out that MAF is favored even in water, against the experimental results (χ_{MAC}~ 0.6). These tendencies were observed with both basis set (DGDZVP and 6-311++G(d,p)) in DMSO, favoring the formation of MAF.

Table 4 K_T values for ERY and EOS in vacuum, water and DMSO obtained with IEF-PCM and SMD solvent models combined with the UFF, Pauling and SMD-Coulomb atomic radii set using B3LYP/DGDZVP and B3LYP/6-311++G(d,p) levels of theory at 298.15 K.

			ERYTROSIN		EOSIN	
			$K_{Q\text{-}L}$	K_M (10^4)	$K_{Q\text{-}L}$	K_M (10^4)
B3LYP/DGDZVP	WATER	IEF-PCM/UFF	0.217	2198.028	1.717	1415.077
		IEF-PCM/Pauling	0.0031	15.005	*	*
		SMD/Coulomb	0.046	0.420	0.0590	5.086
	DMSO	IEF-PCM/UFF	0.300	8734.296	1.417	3893.333
		IEF-PCM/Pauling	0.0049	64.584	*	*
		SMD/Coulomb	1.169	28973.357	4.353	119745.234
B3LYP/6-311++G(d.p)	WATER	IEF-PCM/UFF	0.0263	121.683	0.199	62.970
		IEF-PCM/Pauling	0.0003	1.428	*	*
		SMD/Coulomb	0.0047	0.0054	0.0056	0.4501
	DMSO	IEF-PCM/UFF	0.0458	121.207	0.291	121.065
		IEF-PCM/Pauling	0.0006	2.687	*	*
		SMD/Coulomb	0.199	564.866	0.615	1216.845
[a]Exp. (water)			0.27	0.41	1.24	0.77
[a]Exp.(70 % DMSO)			5.51	12.89	1.16	0.63

*Not Calculated. [a]Experimental values at 303.15 K

Although there are some mistakes concerning the description of monoanionic species in water, the application of B3LYP/6-311++G(d,p) and B3LYP/DGDZVP furnished information about the protolytic system for ERY and EOS, especially when the basis set DGDZVP was used combined with IEF-PCM/UFF and SMD/Coulomb to describe neutral structures. In general the functional B3LYP furnished more adequate results than M06-2X in the study of K_T. The inconsistence in EOS with the tautomeric equilibrium constants, where the experimental results show MAC as preferential while the computational results pointed out to MAF is discussed in the next section, where the pK_a is calculated by computational methodologies.

pK_a predicted by molecular modeling and analysis of the influence of tautomers

The computational calculation of pK_a applied in ERY and EOS system may be useful for understanding the participation of each neutral and monoanionic tautomer in protolytic equilibria. The computational pK_a for all possible protolytic equilibria considering

each tautomer were calculated using the Equations 5 to 11 and the thermodynamic cycles of Scheme SI-1 and Scheme SI-2. The full results are shown in Elec. Supp. Info., Tables SI-4 and SI-8, for all tested levels of theory and solvation models. However the pK_a depends on all tautomeric species that constitute its specific protolytic form, therefore for accounting the contribution of all tautomers it is necessary taking their molar fraction. This was done by calculating the weighted average, using the tautomer's experimental molar fractions (Table 3) and the computational pK_a of each possible equilibrium (pK_{a1} and pK_{a2}), according to the equations 12 and 13. The results obtained with all the calculation methods are shown in Table 5, along with the absolute errors in parenthesis (Error = $pK_{a,exp}(303K) - pK_{a,comp}(298K)$).

$$pK_{a1} = \frac{\chi_{NEQ}\left(pK_{a1,NEQ\leftrightharpoons MAC} + pK_{a1,NEQ\leftrightharpoons MAF}\right) + \chi_{NEL}\left(pK_{a1,NEL\leftrightharpoons MAC} + pK_{a1,NEL\leftrightharpoons MAF}\right)}{4} \quad (12)$$

$$pK_{a2} = \frac{\chi_{MAC}\left(pK_{a2,MAC\leftrightharpoons DA}\right) + \chi_{MAF}\left(pK_{a2,MAF\leftrightharpoons DA}\right)}{2} \quad (13)$$

Certainly the temperature difference between the experimental and theoretical data lead to errors associated with all pK_a results, but this was required because the values of $\Delta G^{o}_{sol}(H^+)$ (Equation 6) in water and DMSO only are well established at 298.15 K, while experimental studies were conducted at 303.15 K. Once the temperatures are close, we do not expect large differences.

Among all levels of theory and solvation models, the best results with smaller errors were obtained with B3LYP/6-311++G(d,p) and SMD/coulomb. Probably the triple zeta 6-311G bases set and the inclusion of two diffusion functions helped thermodynamic description and improved results compared to DGDZVP. Noting that the largest errors usually occur in pK_{a2} values, it is clear that the improvement of the results depends on a good description of the anionic species, which explains the good efficiency of 6-311++G(d,p). This effect has been demonstrated in the K_T study, whereas the K_M values were lower at 6-311++G(d,p) than DGDZVP, approaching the experimental value (K_M < 1, Table 4).

Table 5. Computational pK_a calculated with the weighted average at 298.15 K, considering the experimental molar fraction of each tautomer in water and 70 % DMSO at 303.15 K, for some levels of theory and solvation models/ radii sets. The absolute errors related to experimental pK_a values (Table 1) are given in parentheses

				WATER		WATER	DMSO
				IEF-PCM/UFF	IEF-PCM/Paul.	SMD/Coul.	SMD/Coul.
ERYTHROSIN B and ERYMET	**B3LYP / DGDZVP**	ERYMET	$pK_{a\text{-}OH}$	**-2.29** (6.03)	**-0.91** -4.65)	**1.86** (1.88)	**1.18** (3.46)
		ERY	pK_{a1}	**0.60** (1.75)	**0.55** (1.80)	**1.04** (1.31)	**2.66** (1.92)
			pK_{a2}	**1.45** (3.13)	**1.25** (2.54)	**1.78** (2.01)	**5.10** (0.83)
	B3LYP / 6-311++G(d,p)	ERYMET	$pK_{a\text{-}OH}$	**0.20** (3.54)	**1.51** (2.23)	**2.88** (0.86)	**3.10** (1.54)
		ERY	pK_{a1}	**1.11** (1.24)	**1.07** (1.28)	**1.86** (0.49)	**2.84** (1.74)
			pK_{a2}	**1.99** (1.80)	**1.89** (1.90)	**2,24** (1.55)	**5.50** (0.43)
	M06-2X / DGDZVP	ERY	pK_{a1}	**-1.72** (4.07)	**-1.95** (4,30)	**-1.45** (3.80)	*
			pK_{a2}	**2.76** (1.03)	**2.61** (1.18)	**3.12** (0.67)	*
	M06-2X / LANL2DZ(d,p)	ERY	pK_{a1}	**1.41** (0.94)	**1.07** (1.28)	**1.59** (0.76)	*
			pK_{a2}	**1.34** (2.45)	**0.98** (2.81)	**1.60** (2.19)	*
	B3LYP / DGDZVP (Proton Exchange Method)	ERY	pK_{a1}	*	*	**3.08** (-0.73)	**4.78** (-0.20)
			pK_{a2}	*	*	**4.11** (-0.32)	**7.52** (-1.59)
	B3LYP / 6-311++G(d,p) (Proton Exchange Method)	ERY	pK_{a1}	*	*	**2.98** (-0.63)	**3.64** (0.94)
			pK_{a2}	*	*	**3.36** (0.43)	**6.96** (-1.03)
EOSIN Y and EOSMET	**B3LYP / DGDZVP**	EOSMET	$pK_{a\text{-}OH}$	*	*	**-1.06** (3.17)	**-1.20** (3.56)
		EOS	pK_{a1}	*	*	**0.71** (1.31)	**14.50** (-12.46)
			pK_{a2}	*	*	**1.47** (2.33)	**-15.27** (-22.34)
	B3LYP / 6-311++G(d,p)	EOSMET	$pK_{a\text{-}OH}$	*	*	**1.85** (0.26)	**1.41** (0.95)
		EOS	pK_{a1}	*	*	**0.84** (1.18)	**1.81** (0.23)
			pK_{a2}	*	*	**2.14** (1.66)	**3.28** (3.79)
	B3LYP / DGDZVP (Proton Exchange Method)	EOS	pK_{a1}	*	*	**2.98** (-0.96)	**16.97** (-14.93)
			pK_{a2}	*	*	**1.87** (1.93)	**-13.06** (20.13)
	B3LYP / 6-311++G(d,p) (Proton Exchange Method)	EOS	pK_{a1}	*	*	**1.67** (0.35)	**3.25** (-1.21)
			pK_{a2}	*	*	**2.97** (0.83)	**4.45** (2.62)

*Not calculated.

RSC Advances

ARTICLE

The comparison between the B3LYP functional and M06-2X, using the same basis set of DGDZVP showed lower errors for B3LYP. The M06-2X/LANL2DZ(d,p) method provided good pK_a results, but the calculation time was much greater than B3LYP with DGDZVP or 6-311 ++ G (d, p) (~ 8 times), and provide poor K_T results, making its usage impracticable in the entire system.

In relation to the solvation methods, the better description of SMD/Coulomb over other solvation models and radii sets should be related to its large parameterization, including with the B3LYP functional.[65] Besides it, SMD considers the electrostatic contribution of the bulk solution as well as the first solvation layer in the calculation of ΔG^{o}_{sol}, which improves the pK_a results. Such as observed in K_T determinations, the Coulomb radii seems to be the main factor to the best performance of SMD, once the inclusion of UFF and Pauling did not exhibit improvements compared to IEF-PCM (Elec. Supp. Info., Table SI-6 and SI-7). Facing such results, IEF-PCM model was not used for the subsequent cases.

The results were still better using the proton exchange method because of the inclusion of a HRef (EOSMET or ERYMET) in the thermodynamic cycle, with less than 1 pK_a unit deviation of experimental results in water. It allows the conservation of charges in both sides of equation and cancelations of some errors generated by continuum solvation methods.[44] The complete results of all possible protolytic equilibrium, considering each tautomer, are in Table 6, obtained with B3LYP/6-311++G(d,p) and SMD/Coulomb through the proton exchange method. Probably, the values in Table 6 are close to the real pK_a of each possible protolytic equilibrium, which contribute to the experimental pK_{a1} and pK_{a2} values. Thus, these results allied to the experimental molar fraction (Table 3) could help to understand the protolytic equilibrium and the pK_a inversion of EOS and ERY in DMSO.

Table 6. pK_a values involving tautomers of ERY and EOS obtained by the **proton exchange method** with B3LYP/6-311++G(d,p) and SMD/Coulomb in water and DMSO, at 298.15 K.

				ERYTHROSIN B		EOSIN Y	
				Water	**DMSO**	**Water**	**DMSO**
B3LYP / 6-311++G(d.p)	pK_{a1}	NEQ⇌MAC	COOH	**6.42**	11.29	6.16	10.46
		NEQ⇌MAF	OH	6.02	5.63	**2.96**	**3.30**
		NEL⇌MAC	OH	5.19	11.47	3.94	9.71
		NEL⇌MAF	OH	4.80	**5.81**	**0.73**	**2.55**
	pK_{a2}	MAC⇌DA	OH	**6.62**	8.65	4.55	6.10
		MAF⇌DA	COOH	7.00	**14.32**	**7.76**	**13.26**
	EXPERIMENTAL			$pK_{a1\text{-}COOH}$=2.35± 0.09 $pK_{a2\text{-}OH}$=3.79± 0.09	*$pK_{a1\text{-}OH}$ = 4.58 ± 0.10 *$pK_{a2\text{-}COOH}$ = 5.93 ± 0.08	$pK_{a1\text{-}OH}$ =2.02 ± 0.05 $pK_{a2\text{-}COOH}$ = 3.80 ± 0.06	*$pK_{a1\text{-}OH}$ = 2.04 ± 0.05 *$pK_{a2\text{-}COOH}$ = 7.07 ± 0.09

ERY in water: From the previous discussions the pK_a of ERY is investigated for two protolytic equilibrium involving NEQ and MAC as the main structures in water solution: NEQ ⇌ MAC ($pK_{a\text{-}COOH}$) and MAC ⇌ DA ($pK_{a\text{-}OH}$), as highlighted in Table 6. For pK_{a2}=$pK_{a\text{-}OH}$ the structural molecular analysis unequivocally demands the MAC involvement and, as a consequence, the pK_{a1} relates to carboxylic-carboxylate $pK_{a\text{-}COOH}$ with MAC formation (Scheme in Fig. 1).

The *implicit-explicit* method of pK_a calculations (Scheme SI-3), including three explicit water molecules and the SMD-Coulomb solvation model, with the B3LYP/DGDZVP method, resulted a similar value for NEQ⇌ MAC ($pK_{a1\text{-}COOH}$= 6.6), but a discrepant result for MAC⇌DA ($pK_{a2\text{-}OH}$= 4.4) of ERY. For EOS, the $pK_{a1\text{-}OH}$= -45.6 was not suitable for NEQ⇌MAF and for MAF ⇌ DA the the $pK_{a2\text{-}COOH}$= 4.4. Only these two equilibria for ERY and EOS were performed with this solvation method, but the results do not indicate a real improvement in relation to the implicit solvation methods. Moreover, the explicit water molecules enhanced a lot of the time machine to continue the study with it.

ERY in DMSO: For ERY in DMSO the focused equilibrium are NEL ⇌ MAF, pK_{a1} ($pK_{a\text{-}OH}$) and MAF ⇌ DA, pK_{a2} ($pK_{a\text{-}COOH}$) that corresponds to $pK_{a\text{-}OH} < pK_{a\text{-}COOH}$ (Table 6, highlighted), according with molar fraction observed in Table 3. It is worth to remember that the direct transformation NEL to MAF is structurally impracticable, as already mentioned. Despite it, the computational calculations permits evaluation of NEL ⇌ MAF once we are interested only in the pK_a value of acid-basic equilibrium between these most representative tautomers.

In vacuum (Table SI-6) an expressive pK_a elevation is noted for all equilibria of ERY and ERYMET once ions stabilization is not favored, leading to low acidity and consequently high pK_a.[66] This tendency is confirmed experimentally and theoretically by the results of ERY in 70% DMSO, which pK_a are higher than in water.

EOS in water-DMSO: The involvement of MAF leading to pK_{a2} associated to MAF ⇌ DA, $pK_{a\text{-}COOH}$, is evident for systems where $pK_{a\text{-}OH}<pK_{a\text{-}COOH}$. However, doubts exist concerning the pK_{a1} ($pK_{a\text{-}OH}$). From Table 3, NEL and NEQ are in similar amounts in water. But in

Table 6, the $pK_{a\text{-}OH}$= 2.96 for NEQ⇌MAF is bigger than $pK_{a\text{-}OH}$= 0.73 for NEL⇌MAF, indicating a major contribution of NEQ to the experimental pK_{a1}= 2.02 value of EOS. Also again, it is worth considering the steps hypotheses of NEL → NEQ →→ MAF (as previously discussed), which furnished $pK_{a\text{-}OH}$<$pK_{a\text{-}COOH}$ (as the experimental findings). This same analyses is possible in DMSO, but with less confidence due to higher errors obtained in Table 5.

Despite prevalence of MAC of EOS in all water/DMSO mixtures (χ_{MAC}~ 0.6, Table 3), once again the proposition of MAC as the reason for pK_a inversion is not correct because of structural concerns ($pK_{a2\text{-}COOH}$ is only possible with MAF). Furthermore, the computational pK_{a2} values for MAC ⇌ DA in water and DMSO are considerable smaller than MAF ⇌ DA (Table 6). Then, even the small amount of MAF (χ_{MAF}~ 0.40) justify the experimental findings of pK_{a2} of EOS.

The comparative computational analysis on the acidity of –OH substituent in water between ERY and EOS shows that the $pK_{a\text{-}OH}$ of EOS is lower than the value of ERY, which agreed with the experiments (Tables 1 and 5), while for $pK_{a\text{-}COOH}$, there is not this tendency. Similar results were also obtained with ERYMET and EOSMET ($pK_{a\text{-}OH}$). The higher –OH acidity of EOS and EOSMET than ERY and ERYMET is attributed to the higher bromine electronegativity than iodine atoms.[51,67]

Natural Bond Orbitals Analysis: electronic delocalization energy

Beyond charge density distribution and hydrogen bonding effects, other parameters can affect the molecule's stability in equilibrium. In the present case, the electronic delocalization energy (E_{del}) is included between bonding and antibonding orbitals, which depend on the solvation process. By applying Natural Bonding Orbitals (NBO) analysis, this energy can be calculated for each solvent.[68] If only this effect is considered, high E_{del} means high resonance and better stabilization of the compound in this environment by the solvent molecule's solvation.

MAF of ERY and EOS: The E_{del} calculated for MAF of ERY (Table 7), despite being very high, did not show significant differences in DMSO and in water. For EOS the MAF values are lower than for ERY and once again, no E_{del} difference was detected between DMSO and water as solvent. For MAF the small E_{del} changes with the solvent are due to the intrinsic charge distribution in its structure, which is homogeneously distributed over the entire xanthene ring.

MAC of ERY: from water to DMSO the E_{del} increased by +17320 kcal/mol for MAC of ERY, while for MAF of ERY this value increased only by +181 kcal/mol. The MAC lower E_{del} than MAF in water incorrectly suggests preference of MAF, however the experimental results demonstrated the opposite (χ_{MAC}= 0.71 in water, Table 3). Therefore, in water the stability of the monoanionic tautomer is not driven by the electronic delocalization energy, and in some ways the found inconsistence reflects the major influence of the dipole and hydrogen bonding interactions on MAC stability. In DMSO the E_{del} for MAF higher than MAC justifies the high amount of MAF in the equilibrium as the experimental findings in 70% of DMSO (χ_{MAF}= 0.93 while χ_{MAC}= 0.07, Table 3).

EOS: for MAC of EOS the difference from water to DMSO is -14244 kcal/mol, while for MAF, it is +116 kcal/mol. Therefore the delocalization energy of MAC/EOS diminishes from water to DMSO, showing the low relevancy of this parameter to MAC stabilization in DMSO, once experimentally χ_{MAC} is slightly higher than χ_{MAF} independently of DMSO percentage in water.

Table 7 Electronic delocalization energy (E_{del}) obtained from NBO using B3LYP/DGDZVP with SMD-Coulomb in water and DMSO.

	E_{del} ERY (kcal/mol)		E_{del} EOS (kcal/mol)	
	Water	DMSO	Water	DMSO
MAC	23534.3	40853.9	34064.0	19819.7
MAF	46329.4	46510.5	26540.8	26656.5

Natural Bond Orbitals Analysis: orbital interactions

One important factor that contributes to the presence of MAF of ERY in water is the higher delocalization resonance (high E_{del}) than EOS and the overlap among σ bonding orbitals (donors) of C–I bonding with π* antibonding orbitals (acceptors) of C–C bonding of the xanthene. From energy calculation utilizing second-order perturbation theory were obtained the energies of hyperconjugative interaction corresponding to the orbital overlapping.[68,69] These values can be nominated as electronic stabilization energy (E_{stab}), listed in Table SI-9 of Elec. Supp. Info. for the most significant interactions involving σ of C-X (with X=Br or X=I) and π* of C–C orbitals, as exemplified in Fig. 6A between σ of C2–X20 and π* orbitals of C1–C13 and of C3–C4. The results obtained for the most significant interactions varied from 4.42 to 5.97 kcal/mol for EOS and from 5.77 to 7.24 for ERY. As higher the E_{stab}, greater is the overlap of orbitals, which allows an extensive electronic delocalization.[68,70] As observed for ERY the values of E_{stab} are higher than for EOS.

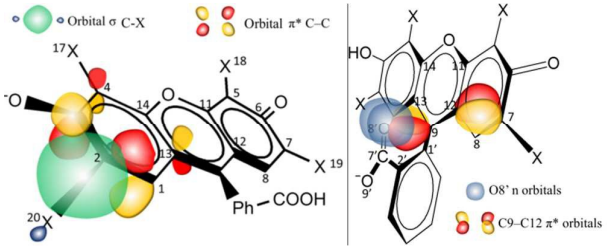

Fig. 6 Schematic illustration of the orbital interaction in ERY (X=I) and EOS (X=Br): **(A)** σ bonding orbital of C2–X20 bond with the antibonding π* orbitals of C1–C13 and of C3–C4 at MAF structure; **(B)** non-bonding (n) of the O8' of carboxylic group with antibonding π* orbital of C9–C12 for MAC structure. The atom numeration follows the IUPAC norms.

From NBO calculation the polarization suffered in the C–I bond of ERY and C–Br bond of EOS were also analyzed in terms of perceptual localization of the bond electron pair on each atom (Elec. Supp. Info., Table SI-10). For EOS the four C–Br bonds show the average polarization values of: C–Br as 47.8–52.2% for MAC and C–Br as 47.0–53.0% for MAF. So the C–Br bonds are negatively polarized on the bromine atom leaving the carbon with positive density, as expected, because bromine (2.96) presents higher Pauling electronegativity than the carbon (2.55).[51] However for ERY, despite the high electronegativity of iodine (2.66), which is slightly

higher than the carbon, the averaged values were: C–I as 55.3%–44.7% for MAC and 54.2%–45.8% for MAF. Which means for C–I bond the negative charge is displaced to carbon atoms instead of the iodine probably due to atomic radius (r) difference which is $r_I > r_{Br}$. The large σ orbital of C–I exhibits high overlapping toward π* of C–C that contributes to higher E_{stab} of ERY than EOS.

The Fig. 6B illustrates interactions among two non-bonding electron pairs – "n" lone pair of O8' – and antibonding orbitals of the xanthene ring, founded in NBO results. This will be discussed ahead.

Evaluation of the computational approach better suited to describe the electronic absorption spectra

Some levels of theory were tested to obtain the better correlation between TD-DFT and experimental spectra, including B3LYP, CAM-B3LYP and M06-2X, cited as good functionals for UV spectra of benzoic acid derivatives[71] (Table 8 and Table SI-11). However apparently the results are very dependent of the basis set, whose use is limited by the presence of iodine and bromine atoms. The better correlations were found using B3LYP/6-311++G(d,p) and SMD/Coulomb, as showed in Table 8 with the λ_{max} for the most representative HOMO→LUMO transition (with the highest transition coefficient) and the respective harmonic oscillator strength (*f*) for each species studied. For all theory levels, the theoretical λ_{max} were lower than the experimental values, whose problem can occur in TD-DFT methods for evaluation of excitation energies.[72,73] The neutral ERYMET-NE showed λ_{max} shift of ~30 nm ($\Delta\nu$ ~0.4 s^{-1}), while the monoanionic ERYMET-MA and dianionic DA are shifted about ~65nm ($\Delta\nu$ ~ 0.9 s^{-1}) comparing with experimental values (Table 2 and Table SI-11). This higher deviation for anionic species probably is caused by the impossibility to add diffuse function for all atoms and also the polarization functions that are not sufficient to describe correctly chemical bonds involving large atoms as bromine and iodine.[74]

For easy comparison between the theoretical and experimental spectra (this obtained by Matrix-K methodology), Fig. 7, the main transitions in water and DMSO are presented for neutral tautomers NEQ and NEL and the monoanionic MAC and MAF of ERY (and in Fig. SI-2 for EOS). It is worth to mention that the *f*= 1 is the superior limit of electronic transitions that is equivalent to an absorptivity of $1x10^5$ L mol^{-1} cm^{-1} (the inferior limit is *f*= 0.01).[75,76] Therefore the spectra are presented with *f* from 0 to 1 and the experimental spectra from 0 to $1x10^5$ L mol^{-1} cm^{-1}.

NEL and NEQ: For the neutral tautomer NEL of both ERY and EOS in water and in DMSO, the significant *f* values are shown only in the UV region that confirms f_{NEL}= 0 in the visible region. Therefore the experimental spectrum of NE corresponds to the NEQ where two main peaks are observed in the visible region independent of the solvent (Figs. 8A and 8C).

MAC and MAF of ERY in water: The lower *f* of MAC compared to MAF justifies the low experimental absorptivity of the monoanionic species of ERY/water in Table 2 allied to the result in Table 3 that shows, despite the low absorptivity, high presence of MAC, χ_{MAC}= 0.71 in water. MAF presents λ_{max} of 17 nm higher than MAC (Table 8), therefore the experimental band at 529 nm probably corresponds to MAF while the shoulder at ~490 nm to MAC. Indeed we reinforce again that, despite the fact that MAC showed lower absorbance intensity (Fig. 7B), it is the preferred tautomer in water (Table 3).

MAC and MAF of ERY in DMSO: In the experimental spectrum of monoanionic species in DMSO the MAF peak showed up on the right side with very high absorption intensity, while the MAC's small peak is present in the blue-shift region (Fig. 7D). This large intensity difference between the experimental absorptivities of MAF and MAC can not be only justified by the difference in *f* values, although for MAC *f* is 43% of the MAF (Table 8 and Fig. 7D). In fact the results are consistent with a higher proportion of MAF in this tautomeric equilibrium, such as χ_{MAF}= 0.93 in 70% DMSO (Table 3).

Table 8 HOMO→LUMO transitions, wavelength of the maximum absorption peak (λ_{max}) and the oscillator strength (*f*) for protolytic and tautomeric forms of ERY, ERYMET, EOS and EOSMET in water and DMSO obtained from B3LYP/6-311++G(d.p) and SMD-Coulomb.

	ERYTROSIN								EOSIN							
	Water				DMSO				Water				DMSO			
	λ_{max} (nm)	Orbitals*	Trans. Coef.	*f*	λ_{max} (nm)	Orbitals*	Trans. Coef.	*f*	λ_{max} (nm)	Orbitals*	Trans. Coef.	*f*	λ_{max} (nm)	Orbitals*	Trans. Coef.	*f*
NEQ	463	H→L H-1→L	0.64 0.30	0.34	462	H→L H-1→L	0.65 0.27	0.39	447	H→L H-1→L	0.64 -0.28	0.36	449	H→L H-1→L	0.65 -0.26	0.38
NEL	270	H→L+4 H→L+5 H-2→L+3	0.47 0.26 0.20	0.37	270	H→L+4 H→L+5 H-2→L+4	0.48 0.22 0.22	0.42	261	H→L+4 H-2→L+3 H-3→L+1	0.43 0.19 0.15	0.36	262	H→L+4 H-2→L+5 H→L+7	0.40 0.19 0.13	0.36
MAC	450	H→L H-1→L	0.65 0.26	0.39	456	H→L H-1→L H-2→L	0.67 -0.14 -0.11	0.39	440	H→L H-1→L	0.66 -0.23	0.40	458	H→L H-1→L	0.64 -0.27	0.25
MAF	468	H→L	0.70	0.87	472	H→L	0.70	0.90	459	H→L	0.70	0.83	463	H→L	0.71	0.84
DA	461	H→L	0.70	0.84	461	H→L	0.70	0.86	453	H→L	0.70	0.80	456	H→L	0.70	0.81
MET-NE	462	H→L H-1→L	0.64 0.30	0.34	460	H→L H-1→L	0.65 -0.26	0.39	446	H→L H-1→L	0.64 0.27	0.36	447	H→L H-1→L	0.65 0.25	0.39
MET-MA	468	H→L	0.70	0.85	471	H→L	0.70	0.90	459	H→L	0.70	0.82	463	H→L	0.70	0.84

* H=HOMO; L=LUMO

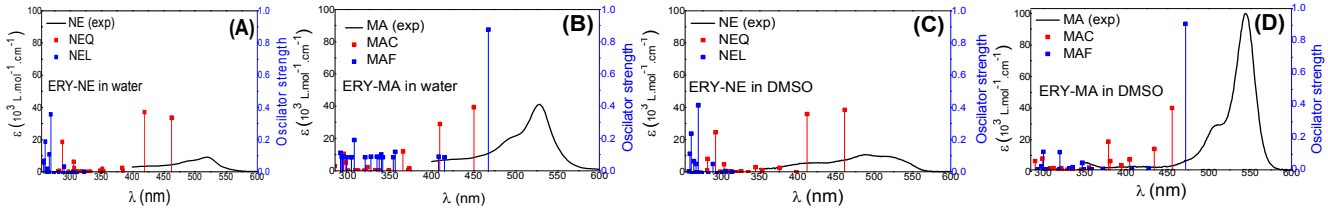

Fig. 7 Absorption spectra for the tautomer forms of neutral (NE) and monoanionic (MA) species determined experimentally using chemometry and estimated by TD-DFT using B3LYP/6-311++G(d,p) with SMD-Coulomb: (A) ERY-NE in water; (B) ERY-MA in water; (C) ERY-NE in DMSO; (D) ERY-MA in DMSO.

MAC and MAF of EOS in water: The theoretical results for EOS in water (Table 8 and Fig. SI-2B) show f_{MAC}= 0.828 higher than f_{MAF}= 0.404 and $\lambda_{max,MAF}>\lambda_{max,MAC}$, similarly as verified for ERY. Therefore for the experimental spectrum of monoanionic species, the peak on the right side belongs to MAF, while the small shoulder on the left side is related to MAC. The intensities of these experimental peaks is coherent with the almost equivalent presence of both tautomers, as experimentally calculated, χ_{MAF}= 0.43 and χ_{MAC}= 0.57 (Table 3).

MAC and MAF of EOS in DMSO: For monoanionic species of EOS in DMSO also again as in water f_{MAF} is lower than f_{MAC} (Fig. SI-2D) and the amount of MAF and MAC should be similar (χ_{MAF} = 0.39).

Additionally the theoretical data in Table 8 confirms that MAF, DA and MET-MA (methyl ester) for ERY and EOS – the phenolate chromophore structure, exhibit similar characteristics among them: the orbitals participating in the HOMO→LUMO transition and the molar absorptivities. The same similarity was verified among NEQ, MAC and MET-NE (methyl ester) for ERY and EOS – the phenolic chromophore structure. Particularly the oscillator strength showed: $f_{MAF} \sim f_{DA} \sim f_{MET\text{-}MA}$ and $f_{NEQ} \sim f_{MAC} \sim f_{MET\text{-}NE}$ in water and DMSO that confirms the approaches used for the molar fractions and tautomeric constant determinations: $\varepsilon_{MAF} = \varepsilon_{DA} = \varepsilon_{MET\text{-}MA}$ and $\varepsilon_{NEQ} = \varepsilon_{MAC} = \varepsilon_{MET\text{-}NE}$. As shown the TD-DFT results seems appropriate and reinforce the approximations adopted leading to confident calculation of molar fractions and tautomeric constants (Table 3).

In spite of these similarities, there are some differences between MAC to NEQ and MET-NE (ester) and DA to MAF and MET-MA (ester). For example f_{MAC} was around ±0.05 units different from f_{NEQ} and $f_{MET\text{-}NE}$ (expect for ERY in DMSO). However these errors are not enough to affect significantly the K_M determinations (Table 3), or to cause prejudice to the qualitative analysis of the protolytic equilibria. These differences are discussed in the next item.

HOMO-LUMO transitions and the charge effect of the carboxylate on the chromophore group

As observed in Table 8, the HOMO→LUMO are the most significant electronic transitions for the structures of ERY and EOS. Note that for MAC, NEQ and MET-NE, the involved orbital (H→L) resulted to very close values of λ_{max}. The same effect occurs among DA, MAF and MET-MA. In NEL, the only exception, the high difference of energy between HOMO and LUMO+4 (Table 8) makes the transition to occur at the UV, instead of visible region.

As exemplified using MAC and MAF, the delocalization of the electronic density occurs from the borders of the chromophoric region of the HOMO toward the central xanthene ring of LUMO, Fig. 8. Besides, from observing the high orbital π overlapping of the xanthene part, the transition HOMO→LUMO involves mainly orbitals π→π*, which are consistent with the region at ~500 nm.[59,76,77]

As already mentioned, despite the similarity of the chromophoric groups and spectra, some differences showed up (Table 8) for DA in relation to MAF and MET-MA and MAC in relation to NEQ and MET-NE. It is worth mentioning that both DA and MAC present the carboxylate group (–COO^-). It is already reported for ERY that, despite no significant interference to molar absorptivity, the substituent –COO^- could influence the xanthene chromophore ring causing spectral differences up to 10 nm in λ_{max} between DA and MAF.[78] In our previous study[13] with Fluorescein it was concluded that, although the negative charge on the carboxylate in DA causes the increase of the benzene ring's resonance, it participates minimally to the resultant main electronic transitions. It is important to emphasize that effect occurs without the direct resonance between the xanthene part with the benzene ring due to the orthogonality[9,13] as illustrated in Fig. 5, Fig. 7B and Fig. SI-1. Therefore it suggests the occurrence of intramolecular interactions involving orbitals from –COO^- and xanthene part.

To investigate this effect, the specific interactions at NBO of O7' and O9' with atoms of the xanthene ring were studied). The significant stabilization energies (E_{stab}> 0.50 kcal/mol) was found among NBO of two non-bonding electron pairs – "n" lone pair of O8' – and antibonding orbitals of the xanthene ring, as illustrated previously in Fig. 7B for MAC between n (O8') and π* (C9–C12).

For ERY the E_{stab} of MAC (7.82 kcal/mol) was higher than the value for NEQ (2.18 kcal/mol) and MET-NE (2.17 kcal/mol). The same occurred for EOS, with the E_{stab} values of MAC (7.88 kcal/mol), NEQ (2.21 kcal/mol) and MET-NE (2.35 kcal/mol). Similarly for ERY the E_{stab} resulted for DA (9.90 kcal/mol) much higher than MAF (4.10 kcal/mol) and MET-MA (4.37 kcal/mol), and for EOS the DA (9.61 kcal/mol) was much higher than MAF (4.05 kcal/mol) and MET-MA (4.27 kcal/mol).

Thus, these higher values of E_{stab} for MAC with NEQ and MET-NE and for DA with MAF and MET-MA pointed out effective interaction between n orbitals of O8' with xanthene ring orbitals for MAC and DA, which have the carboxylate group -COO^-. The other structures that present –COOH or –$(COO)CH_3$ (the esters) show weak orbital overlapping due to the absence of the negative charge. Therefore these interactions justify the spectral differences observed by the presence of the carboxylate group on the electronic delocalization

of the chromophore causing the results observed in λ_{max} and molar absorptivities listed in Table 8.

These orbital's interactions are also evidenced in the side view of HOMO and LUMO (Fig. 8). The HOMO of $–COO^-$ for MAC is large enough to overlap the LUMO of the xanthenes suggesting effective participation on the electronic transition. This phenomenon, allied to differences at the chromophoric group of MAC and MAF, caused a shift of more than 15 nm ($\Delta\nu \sim 0.2\ s^{-1}$) in the λ_{max} of these species (Table 8). On the other hand, there is no HOMO of the -COOH in MAF to overlap to LUMO of the xanthene's orbitals. Consequently, there is not a HOMO→LUMO transition.

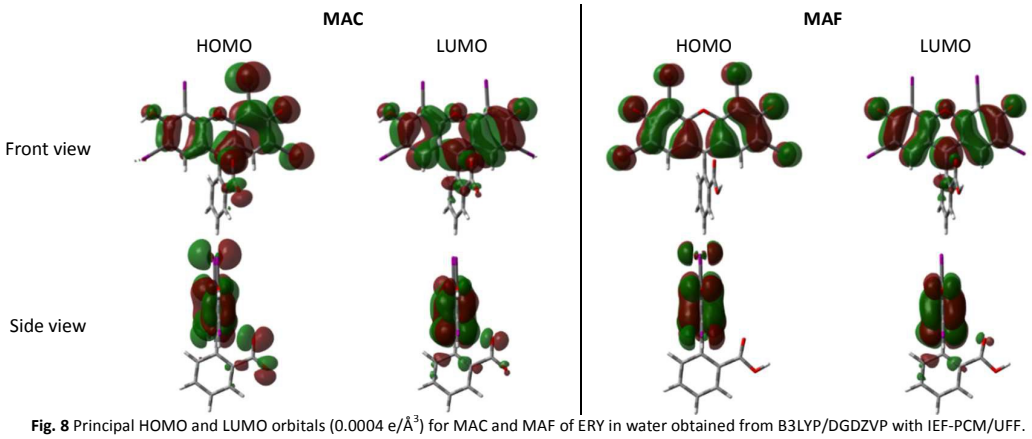

Fig. 8 Principal HOMO and LUMO orbitals (0.0004 e/Å^3) for MAC and MAF of ERY in water obtained from B3LYP/DGDZVP with IEF-PCM/UFF.

Conclusions

In general the experimental tautomeric equilibrium constants for ERY show that the most representative sequence of protolytic equilibria in water rich media is NEQ ⇌ MAC ⇌ DA, while above 35% of DMSO in water is NEL ⇌ MAF ⇌ DA. For EOS, there are two possibilities: NEL ⇌ MAF or NEQ ⇌ MAF as pK_{a1}=$pK_{a\text{-}OH}$ and MAF ⇌ DA as pK_{a2}=$pK_{a\text{-}COOH}$ in the range of 0 to 70 % of DMSO in water. The lower dielectric solvent constant in water/DMSO mixtures causes the pK_a inversion for ERY due to the high ratio MAF/MAC and NEL stabilization. Therefore, this is not only NEL prevalence that commands the pK_a inversion, but mainly MAC and MAF.

The high dipole moment with charge polarity of NEQ and MAC of ERY justifies their stabilization in water, while the high charge distribution over the entire molecule of MAF permits high stabilization in solvents with low dielectric constants (compared to water), such as in DMSO. However particularly MAF of EOS presents a high dipole moment that contributes to its reasonable stability in water, which explains the $pK_{a–OH} < pK_{a–COOH}$ independent of the DMSO presence. This effect is originated from the electronic delocalization differences of MAF for ERY and EOS, influenced for the overlap between the NBO σ orbitals of C–I (ERY) or of C–Br (EOS) with π* of C–C, in which for ERY is higher than for EOS.

The spectrum of each tautomer form simulated with TD-DFT permitted to confirm the experimental finds of molar fractions, and that the statement of $\varepsilon_{MET\text{-}NE}$= ε_{NEQ}= ε_{MAC} and $\varepsilon_{MET\text{-}MA}$= ε_{MAF} is adequate leading to confident K_T values. The NBO and HOMO-LUMO orbitals confirm that the negative charge of $–COO^-$ causes a small influence on the xanthene chromophore caused by the interaction of n-π* orbitals.

All results allowed for a better comprehension of the pK_a inversion and the prediction of the tautomer's participation on ERY and EOS equilibria combined with the solvent dependence. These results contribute to several applications such as photosensitizers in PDT and PDIMO, once permitted to drive the structure's presence and its properties under light.

Acknowledgements

This work was sponsored by the Brazilian funding agencies UGF-SETI/PR, CAPES, FAPEMIG and CNPq.

References

1 A. Savino and G. Angeli, *Wat. Res.*, 1985, **19**, 1465-1469.
2 S. Wood, D. Metcalf, D. Devine, C. Robinson, *J. Antimicrob. Chemother.*,2006, **57**, 680-684.
3 J. Y. Nagata, N. Hioka, E. Kimura, V. R. Batistela, R. S. T. Terada, A. X. Graciano, M. L. Baesso and M. F. Hayacibara, *Photodiag. Photodyn. Ther.*, 2012, **9**, 122-131.
4 D. S. Pellosi, V. R. Batistela, V. R. Souza, I. S. Scarminio, W. Caetano and N. Hioka, *Ann. Braz. Acad. Sci.*, 2013, **85**, 1267-1274.
5 B. M. Estevão, D. S. Pellosi, C. F. Freitas, D. Vanzin, D. S. Franciscato, W. Caetano and N. Hioka, *J. Photochem. Photobiol. A Chem.*, 2014, **287**, 30-39.
6 N. N. Yassunaka, C. F. Freitas, B. R. Rabello, P. R. Santos, W. Caetano, N. Hioka, T. U. Nakamura, B. A. Abreu Filho and J. M. G. Mikcha. *Curr Microbiol.*, 2015, **71**, 243-251.
7 L. S. Herculano, G. V. B. Lukasievicz, E. Sehn, W. Caetano, D. S. Pellosi, Noboru Hioka, , N. G. C. Astrath and L. C. Malacarne. Appl. Spectrosc., 2015, **69**, 883-888.
8 N. O. Mchedlov-Petrossyan and R. S. Mayorga, *J. Chem. Soc. Far. Trans.*, 1992, **88**, 3025-3032.
9 Y. H. Jang, S. Hwang and D. S. Chung,*Chem. Lett.* 2001, **30**, 1316-1317.
10 N. O. Mchedlov-Petrossyan, N. A. Vodolazkaya, Y. N. Surov and D. V. Samoylov, *Spect. Acta Part A*, 2005, **61**, 2747-2760.

11 N. A. Vodolazkaya, P. V. Shakhova and N. O. Mchedlov-Petrossyan, *Russ. J. Gen. Chem.***,** 2009, **79**, 1437-1445.
12 N. A. Vodolazkaya, Y. A. Gurina, N. V. Salamanova and N. O. Mchedlov-Petrossyan, *J. Mol. Liq.*, 2009, **145**, 188-196.
13 V. R. Batistela, J. C. Cedran, H. P. M. Oliveira, I. S. Scarminio, L. T. Ueno, A. E. H. Machado and N. Hioka, *Dyes and Pigments,* 2010, **86**, 15-24.
14 N. O. Mchedlov-Petrossyan, T. A. Cheipesh, S. V. Shekhovtsov, A. N. Redko,V. I. Rybachenko, I. V. Omelchenko and O. V. Shishkin, *Spec. Acta Part A, Mol. Biomol. Spec.*, 2015, **150**, 151–161.
15 V. R. Batistela, D. S. Pellosi, F. D. Souza, W. F. Costa, S. M. O. Santin, V. R. Souza, W. Caetano, H. P. M. Oliveira, I. S. Scarminio and N. Hioka, *Spec. Acta Part A,* 2011, **79**, 889-897.
16 N. O. Mchedlov-Petrossyan and V. N. Kleshchevnikova, *J. Chem. Soc. Far. Trans.*, 1994, **90**, 629-640.
17 R. Markuszewski and H. Diehl, *Tatanta*, 1980, **27**, 937.
18 U. Anthoni, C. Christophersen, P. H. Nielsen, A. Püschl, K. Schaumburg, *Struc.Chem*., 1995, **6**, 161.
19 N. O. Mchedlov-Petrossyan, V. I. Kukhitk and S. I. Egorova, *Russ. J. Gen. Chem.*,2006, **76**, 1607-1617.
20 N. O. Mchedlov-Petrossyan, N. V. Salamanova, N.A. Vodolazkaya, Y.A. Gurina and V.I. Borodenko,*J. Phys. Org. Chem.*,2006, **19**, 365-375.
21 M. B. Gholivand, J. B. Ghasemi, S. Saaidpour and A. Mohajerd, *Spec. Acta A,* 2008, **71**, 1158-1165.
22 R. G. Bates, *Determination of pH. Theory and practice*. New York, Wiley, 1964.
23 D.C. Neckers, *J. Chem. Educ.*, 1987, **64**, 649–656.
24 A. V. Lebed, A. V. Biryukov and N. O. Mchedlov-Petrossyan. *Chem. Heterocycl. Comp.*,2014, **50**, 336-348.
25 M. Król, M. Wrona, C. S. Page and P. A. Bates, *J. Chem. Theory Comput.*, 2006, **2**, 1520-1529.
26 D. S.Pellosi, B. M. Estevão, C. F. Freitas, T. M. Tsubone, W. Caetano and N. Hioka, *Dyes and Pigments*,2013, **99**, 705-712.
27 A. J. Cohen, P. Mori-Sánchez and W. *Chem. Rev.*, 2012, **112**, 289-320.
28 N. Godbout, D.R. Salahub, J. Andzelm and E. Wimmer, *Can. J. Chem.*,1992, **70**, 560-571.
29 C. Sosa, J. Andzelm, B. C. Elkin, E. Wimmer, K. D. Dobbs and D. A. Dixon, *J. Phys. Chem.*,1992, **96**, 6630-6636.
30 C.E. Check, T.O. Faust, J.M. Bailey, B.J. Wright, T.M. Gilbert and L.S. Sunderlin, *J. Phys. Chem. A*, 2001, **105**, 8111.
31 M.N. Glukhovstev, A. Pross, M.P. McGrath and L. Radom, *J. Chem. Phys*, 1995, **103**, 1878.
32 J. Tomasi, B. Mennucci and E. Cancès, *J. Mol. Struc.*, 1999, **464**, 211.
33 A. V. Marenich, C. J. Cramer and D. G. Truhlar, *J. Phys. Chem. B*,2009, **113***,* 6378.
34 L. Pauling. The Nature of the Chemical Bond, **3** ed., Ithaca, NY, Cornell University Press, 1960.
35 A. K. Rappe, C. J. Casewit, K. S. Colwell, W. A. Goddard and W. M. Skiff, *J. Am. Chem. Soc.* 1992, **114**, 10024.
36 S. Simon, M. Duran and J. J. Dannenberg, *J. Chem. Phys.*, 1996, **105**, 11024-11031.
37 Gaussian 09, Revision A.01, M. J. Frisch, G. W. Trucks, H. B. Schlegel, G. E. Scuseria, M. A. Robb, J. R. Cheeseman, G. Scalmani, V. Barone, B. Mennucci, G. A. Petersson, H. Nakatsuji, M. Caricato, X. Li, H. P. Hratchian, A. F. Izmaylov, J. Bloino, G. Zheng, J. L. Sonnenberg, M. Hada, M. Ehara, K. Toyota, R. Fukuda, J. Hasegawa, M. Ishida, T. Nakajima, Y. Honda, O. Kitao, H. Nakai, T. Vreven, J. A. Montgomery, Jr., J. E. Peralta, F. Ogliaro, M. Bearpark, J. J. Heyd, E. Brothers, K. N. Kudin, V. N. Staroverov, R. Kobayashi, J. Normand, K. Raghavachari, A. Rendell, J. C. Burant, S. S. Iyengar, J. Tomasi, M. Cossi, N. Rega, J. M. Millam, M. Klene, J. E. Knox, J. B. Cross, V. Bakken, C. Adamo, J. Jaramillo, R. Gomperts, R. E. Stratmann, O. Yazyev, A. J. Austin, R. Cammi, C. Pomelli, J. W. Ochterski, R. L. Martin, K. Morokuma, V. G. Zakrzewski, G. A. Voth, P. Salvador, J. J. Dannenberg, S. Dapprich, A. D. Daniels, O. Farkas, J. B. Foresman, J. V. Ortiz, J. Cioslowski, and D. J. Fox, *Gaussian, Inc.*, Wallingford CT, 2009.
38 ChemDraw Ultra®, *Chemical Structure Drawing Standard: CambridgeSoft Corporation*. Cambridge, MA, 1985-2001. Obtained at www.cambridgesoft.com.
39 J. W. Ochterski, *Thermochemistry in Gaussian*. Gaussian, 2000. Hyperlink: http://www.gaussian.com/g_whitepap/thermo/thermo.pdf, accessed in may/2013.
40 N. Marchand-Geneste and A. Carpy. *J. Mol. Struc. (Theochem)*, 1999, **465**, 209-217.
41 P.U. Civcir. *J. Mol. Struc. (Theochem)*, 2001, **535**, 121-129.
42 I. N. Levine, *Physical Chemistry*, 6 ed., New York, McGraw-Hill, Inc., 2009.
43 M. D. Liptak, K. C. Gross, P. G. Seybold, S. Feldgus and G. C. Shields, *J. Am. Chem. Soc.*, 2002, **124**, 6421-6427.
44 J. Ho and M. L. Coote. *Theor. Chem. Acc.,* 2010, **125**, 3-21.
45 M. Król, M. Wrona, C. S. Page, P. A. Bates, *J. Chem. Theo. Comp.*, 2006, **2**, 1520-1529.
46 M. D. Tissandier, K. A. Cowen, W. Y. Feng, E. Gundlach, M. H. Cohen, A. D. Earhart, J. V. Coe and T. R. Tuttle, *J. Phys. Chem. A*,1998, **102**, 7787-7794.
47 T. R. Tuttle, S. Malaxos and J. V.Coe, *J. Phys. Chem. A*, 2002, **106**, 925-932.
48 M. W. Palascak and G. C. Shields, *J. Phys. Chem. A*, 2004, **108**, 3692-3694.
49 D. M. Camaioni and C. A. Schwerdtfeger, *J. Phys. Chem. A,* 2005, ***109,*** 10795-10797.
50 C. P. Kelly, C. J. Cramer and D. G. Truhlar, *J. Phys. Chem. A*, 2006, **110**, 2493-2499.
51 *CRC Handbook of Chem. and Phys*., **88**, D. R. Lide (Ed.), 2007-2008.
52 Y. Marcus, *Pure Appl. Chem.*, 1983, **55**, 977-1021.
53 F. Amat-Guerri, M. M. C. López-Gonzalez, R. Martínez-Utrila and R. Sastre, *Dyes and Pigments,*1990, **12**, 249-272.
54 M. M. Sena, I. S. Scarmínio, K. E. Collins and C. H. Collins, *Talanta,* 2000, **53**, 453-461.
55 D. Almasifar, F. Forghaniha, Z. Khojasteh, J. Ghasemi, H. Shargi and M. Shamsipur, *J. Chem. Eng. Data*, 1997, **42**, 1212-1215.
56 J. Ghasemi, A. Niazi, M. Kubista and A. Elbergali, *Anal. Chim. Acta*. 2002, **455**, 335-342.
57 N. O. Mchedlov-Petrossyan, V. I. Kukhtik and V. D. Bezugliyz, *J. Phys. Org. Chem.*,2003, **16**, 380-397.
58 X.; Wang, M. Song and Y. Long,*J. Sol. State Chem.*, 2001, **156**, 325-330.
59 E. A.; Slyusareva, F. N. Tomilin, A. G. Sizykh, E. Y. Tankevich, A. A. Kuzubov and S. G. Ovchinnikov, *Spectroscopy of Atoms and Molecules*, 2012, **112**, 671-678.
60 P. Mukerjee and D. Ostrow, *Tetrahedron Lett.*,1998, **39**, 422-426.
61 A. Orte, L. Crovetto, E. M. Talavera, N. Boens and J. M. Alvarez-Pez, *J. Phys. Chem. A*, 2005, **109**, 734-747.
62 A. I. M. C. L. Ferreira and M. A. V. R. Silva, *J. Chem. Therm.*, 2013, **59**, 94–106.
63 J. B. Foresman, Æ. Frisch, *Exploring chemistry with electronic structure methods*, 2 ed., Pittsburgh, Gaussian, Inc., 1996.
64 M. Trsic and M.F.S. Pinto. *Química Quântica: Fundamentos e Aplicações,* Barueri, SP, Manole, 2009.
65 A.V. Marenich, C. J. Cramer and D. G. Truhlar, *J. Phys. Chem.* B, 2009, **113***,* 6378-6396.
66 L. Safarik and Z. Stránský, Titrimetric analysis in organic solvents, *Wilson and Wilson's Comprehensive Analytical Chemistry,* vol. 22, Amsterdam, Elsevier Science Publ., 1986.

67 T. L. Brown, H. E. LeMay, B. E. Bursten, C. J. Murphy and P. Woodward, *Chemistry: the central science*, 11 ed, USA, Pearson Prentice Hall, 2009.
68 E. Glendening, C. R. Landis, F. Weinhold, (Eds). *Tutorial on Energetic Analysis with NBO Deletions ($DEL Keylist)*. Theor. Chem. Inst. of the University of Wisconsin. Hyperlink: http://www.chem.wisc.edu/~nbo5/TUT_DEL.HTM, accessed in February/2014.
69 A. Nataraj, V. Balachandran and T. Karthick, *J. Mol. Struc.*, 2013, **1031**, 221-233.
70 J. E. Huheey, E. A. Keiter and R. L. Keiter, *Inorganic Chemistry: principles of structure and reactivity*, 4 ed, New York, HarperCollins Col. Pub., 1993.
71 H-B Guo, F. He, B. Gu, L. Liang, and J. C. Smith, *J Phys. Chem. A*, 2012, **116** (48), 11870-11879.
72 A. Tamulis, J. Tamuliene, M. L. Balevicius, Z. Rinkevicious and V. Tamulis, *Struct. Chem.,* 2003, **14**, 643.
73 M. E. Casida and M. Huix-Rotllant. *Ann. Rev. Phys. Chem.* 2012, **63**, 287–323.
74 Young, D. C. *Computational chemistry: a practical guide for applying techniques to real-world problems*. New York, John Wiley & Sons, 2001.
75 D. C. Harris and M. D. Bertolucci, *Symmetry and spectroscopy: an introduction to vibrational and electronic spectroscopy*. New York, Dover, 1989.
76 N. J. Turro, *Modern molecular photochemistry*, New York, University Science Books, 1991.
77 B. Valeur, *Molecular fluorescence: principles and applications*. Verlag GmbH, Wiley-VCH, 2002.
78 J. Kibblewhite, G .G. Drummond, F. Grieser and P. J. Thistlethwaite, *J. Phys. Chem.,*1989, **93**, 7464.

Graphical Abstract

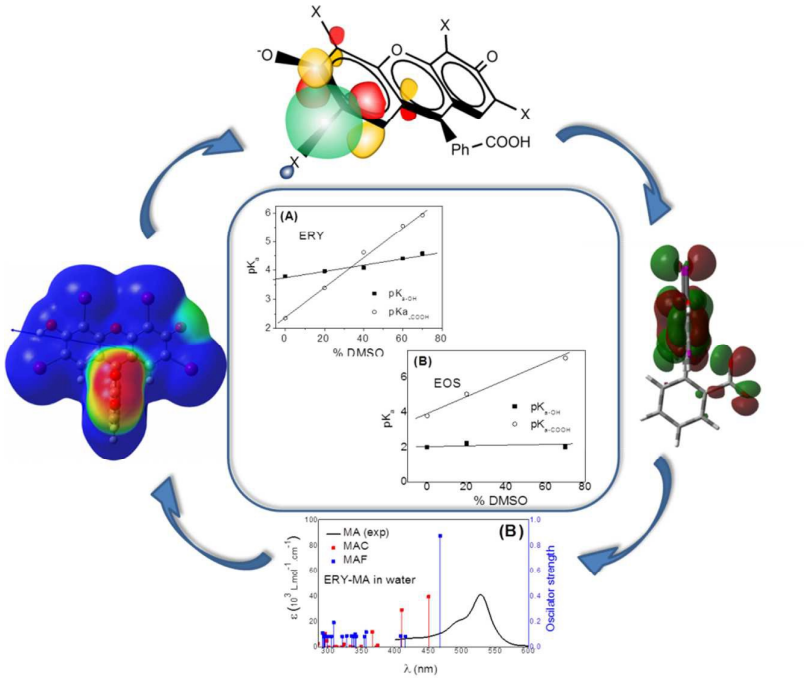

Xanthene dyes Eosin Y (EOS) and Erythrosin B (ERY) are photosensitizers that present complex protolytic system. To understand how the media affects their properties, we correlated the experimental pK_a in water/DMSO with theoretical calculation by molecular modeling approaches based on their tautomer´s energy. It shows that in EOS the phenolic group is more acid than the carboxylic due to the presence of bromine atoms. The iodine in ERY, through the stability of tautomers involved in the protolytic forms, drives $pK_{a\text{-}COOH}<pK_{a\text{-}OH}$ in water-rich media and the inversion $pK_{a\text{-}OH}<pK_{a\text{-}COOH}$ in DMSO-rich media caused by the solvation that affects its tautomeric equilibria. For EOS, the possible protolytic equilibria are: NEL ⇌ MAF or NEQ ⇌ MAF as $pK_{a1}=pK_{a\text{-}OH}$ and MAF ⇌ DA as $pK_{a2}=pK_{a\text{-}COOH}$ in the range of 0 to 70 % of DMSO in water. For ERY at above 35% DMSO in water, the $pK_{a\text{-}OH}<pK_{a\text{-}COOH}$ came from the high amount of MAF and NEL, indicating that these tautomers may be responsible for the inversion. These effects are originated from different electronic delocalization influenced by the overlap between the σ natural bond orbitals of C–I (ERY) or C–Br (EOS) with π* of C–C, higher for ERY than for EOS. The simulated spectra permitted to confirm experimental finds of molar fractions. The analysis of the molecular orbitals confirmed that the main changes in absorption profile are due to HOMO-LUMO π-π* transitions related to the phenolic group. The results allowed the understanding of the influence of environment on preferential tautomers and pK_a.